

# Bulk emission of scalars by a rotating black hole

---

**Marc Casals and Sam Dolan**

*School of Mathematical Sciences, University College Dublin, Belfield, Dublin 4, Ireland.*

*E-mail:* Marc.Casals@ucd.ie, Sam.Dolan@ucd.ie

**Panagiota Kanti**

*Division of Theoretical Physics, Department of Physics, University of Ioannina,*

*Ioannina GR-451 10, Greece*

*E-mail:* pkanti@cc.uoi.gr

**Elizabeth Winstanley**

*School of Mathematics and Statistics, The University of Sheffield, Hicks Building,*

*Hounsfield Road, Sheffield S3 7RH, United Kingdom.*

*E-mail:* E.Winstanley@sheffield.ac.uk

**ABSTRACT:** We study in detail the scalar-field Hawking radiation emitted into the bulk by a higher-dimensional, rotating black hole. We numerically compute the angular eigenvalues, and solve the radial equation of motion in order to find transmission factors. The latter are found to be enhanced by the angular momentum of the black hole, and to exhibit the well-known effect of superradiance. The corresponding power spectra for scalar fields show an enhancement with the number of dimensions, as in the non-rotating case. On the other hand, the proportion of the total (i.e., bulk+brane) power that is emitted into the bulk decreases monotonically with the angular momentum. We compute the total mass loss rate of the black hole for a variety of black-hole angular momenta and bulk dimensions, and find that, in all cases, the bulk emission remains significantly smaller than the brane emission. The angular-momentum loss rate is also computed and found to have a smaller value in the bulk than on the brane.

**KEYWORDS:** Large Extra Dimensions, Black Holes, Beyond Standard Model.

---

## Contents

<b>1. Introduction</b>	<b>1</b>
<b>2. Theoretical background</b>	<b>3</b>
2.1 Scalar field equations	4
2.2 Hawking emission	5
<b>3. Numerical methods</b>	<b>9</b>
3.1 Angular eigenvalues	9
3.2 Transmission factors	10
<b>4. Results</b>	<b>11</b>
4.1 Non-rotating black holes ( $a_d = 0$ )	11
4.2 Rotating black holes, $a_d > 0$	12
4.2.1 Transmission factors	13
4.2.2 Power spectra	15
4.2.3 Angular momentum spectra	19
4.3 Consistency with other studies	22
<b>5. Discussion and conclusions</b>	<b>23</b>

---

## 1. Introduction

Theories with Large Extra Dimensions [1, 2] have proven attractive to theorists in recent years. Of particular interest are models in which matter is confined to a four-dimensional hypersurface (the *brane*), but gravity (and possibly scalar fields) is free to propagate in a higher-dimensional compact space (the *bulk*). Phenomenologically, such models are intriguing because they appear to resolve the so-called hierarchy problem. In other words, they explain why gravity is observed to be so much weaker (on the macroscale) than the other forces.

In these models, the fundamental energy scale of gravity ( $M_*$ ) is related to the Planck energy ( $M_P$ ) by  $M_*^{2+n} \sim M_P^2 R^{-n}$ , where  $R$  and  $n$  are the size and number of extra dimensions. Hence,  $M_*$  may be many orders of magnitude lower than the Planck energy  $M_P$ . This raises the tantalising prospect that black holes may be created through ‘trans-Planckian’ particle collisions [3]. It has been suggested that  $M_*$  may be probed by high-energy cosmic ray collisions [4], or the next generation of particle accelerators [5]. If created, mini black holes would evaporate rapidly through emitting Hawking radiation [6]. Experimental detection of Hawking emission would provide a clear signal of black

hole creation. Accurate measurement of the power spectrum would enable us to deduce the properties of the underlying spacetime itself. For these reasons, accurate theoretical modelling of the emission spectrum has become a high priority, and it has received much attention in recent years.

Black holes are thought to undergo four stages of evaporation: the so-called ‘balding’, ‘spin-down’, ‘Schwarzschild’, and ‘Planck’ phases [7, 8]. Thanks to a number of analytical [9, 10, 11] and numerical [12, 13] studies, emission from the Schwarzschild phase is now well described. Attention has recently shifted to emission in the rotating phase [14, 15, 16, 17].

In this paper, we conduct a numerical study of scalar emission in the bulk by a rotating higher-dimensional black hole. Our work complements a range of existing studies of the ‘spin-down’ phase of black hole evolution. In previous papers in this series we have examined on-the-brane emission of scalars [15], fermions [16] and photons [17] by a rotating black hole. In parallel, other groups have pursued complementary lines of inquiry [18]. The bulk emission of scalars from the rotating phase has received increasing attention. Analytic approximations for the greybody factors (transmission factors) were recently derived [19]. The analytic work is complemented by two recent numerical studies [20, 21] of bulk scalar emission from 5D and 6D rotating holes. Here, we present comprehensive new exact results for bulk dimensionalities  $n = 1, 2, \dots 6$ , and a range of black hole angular momenta.

This study aims to investigate the claim that *black holes radiate mainly on the brane* [22]. Studies of the Schwarzschild phase of evolution found that graviton [13] and scalar [12] emission in the bulk is small compared with emission of standard model fields on the brane, due chiefly to the multiplicity of standard model particle species. Hence, only a small fraction of the black hole energy is ‘lost’ in the bulk. It is widely suspected, but unproven, that the same remains true when the black hole is rotating. As the amount of energy emitted in the bulk inevitably defines the one on the brane – and its observable signatures, this point should be duly clarified. Two species of particles are usually assumed to propagate in the bulk, gravitons and scalars. Whilst it is possible [23] to derive a set of partial differential equations (PDEs) describing the gravitational perturbations of a higher-dimensional rotating black hole, it is not yet clear whether the PDEs can be decoupled into ordinary differential equations (ODEs) for all modes (specifically, the scalar and vector modes) when the black hole has a single angular momentum parameter<sup>1</sup>. On the other hand, in the case of scalars, the decoupling of PDEs is indeed realised, and a comprehensive study of their emission can be performed. Apart from the importance in its own right of the scalar emission, the study of the scalar field in the bulk can also offer a qualitative understanding of higher-dimensional graviton emission from a rotating black hole. In the sections that follow, we compute the strength of scalar emission in brane and bulk channels in the rotating phase, and calculate the proportion of the scalar energy which enters the bulk. We make the assumptions of a minimally-coupled field, negligible brane tension, and a black hole with just one non-zero angular momentum component.

The paper is structured as follows. In section 2 we outline the relevant theory, viz. a mathematical description of a rotating black hole in a bulk spacetime; the decomposition

---

<sup>1</sup>In the case of equal angular momenta, the ODEs have been separated for some modes - see [24] and [25].

of the scalar field into radial and angular parts; and the relevant formulae for Hawking emission. In section 3 the numerical methods employed to calculate angular eigenvalues and transmission factors are described. In section 4 we present our numerical results. We start with a brief review of the Schwarzschild phase results, before moving on to consider the rotating phase. The effect of superradiance on the transmission factors is examined. We present brane and bulk power spectra for a range of  $n$  and black hole angular momenta  $a$ . We compute the total scalar emission rate, and the fraction which is radiated into the bulk. We also consider the loss of angular momentum from the spinning hole. Finally, in section 5 we conclude with a discussion of the physical implications of our work.

## 2. Theoretical background

The well-known Myers-Perry solution [26] describes the gravitational field of a  $(4 + n)$ -dimensional uncharged rotating black hole. We will confine our attention to black holes created by the collision of particles on the brane. Hence we assume that the black hole metric has only one non-zero angular momentum component, in a plane parallel to the brane. The line-element takes the form

$$ds^2 = - \left(1 - \frac{\mu}{\Sigma r^{n-1}}\right) dt^2 - \frac{2a\mu \sin^2 \theta}{\Sigma r^{n-1}} dt d\psi + \frac{\Sigma}{\Delta} dr^2 + \Sigma d\theta^2 + \left(r^2 + a^2 + \frac{a^2 \mu \sin^2 \theta}{\Sigma r^{n-1}}\right) \sin^2 \theta d\psi^2 + r^2 \cos^2 \theta d\Omega_n^2, \quad (2.1)$$

where

$$\Delta = r^2 + a^2 - \frac{\mu}{r^{n-1}}, \quad \Sigma = r^2 + a^2 \cos^2 \theta. \quad (2.2)$$

Here,

$$d\Omega_n^2(\theta_1, \theta_2, \dots, \theta_{n-1}, \phi) = d\theta_{n-1}^2 + \sin^2 \theta_{n-1} \left( d\theta_{n-2}^2 + \sin^2 \theta_{n-2} \left( \dots + \sin^2 \theta_2 \left( d\theta_1^2 + \sin^2 \theta_1 d\phi^2 \right) \dots \right) \right) \quad (2.3)$$

is the line-element on a unit  $n$ -sphere. In equation (2.1), the angle  $\psi$  is the azimuthal angle round the axis of rotation of the black hole in the brane (for four-dimensional black holes, this angle is usually denoted  $\phi$ ). The mass  $M_{BH}$  of the black hole and its angular momentum  $J$  are proportional to  $\mu$  and  $a\mu$ , respectively,

$$M_{BH} = \frac{(n+2)A_{n+2}}{16\pi G} \mu, \quad J = \frac{2}{n+2} M_{BH} a, \quad (2.4)$$

where  $A_{n+2} = 2\pi^{(n+3)/2}/\Gamma[(n+3)/2]$  is the area of an  $(n+2)$ -dimensional unit sphere, and  $G$  is the  $(4+n)$ -dimensional version of Newton's constant. Equation (2.4) effectively defines the parameters  $\mu$  and  $a$  which appear in the metric (2.1).

The radius of the black hole's event horizon,  $r_h$ , is the largest, positive root of  $\Delta(r) = 0$ . The horizon radius  $r_h$  can be employed to define a useful set of dimensionless variables, which we denote with the subscript  $d$ ,

$$r_d = r/r_h, \quad a_d = a/r_h, \quad \omega_d = \omega r_h. \quad (2.5)$$

For  $n \geq 1$ , there is one unique root in the region  $r > 0$ , and it can be obtained from the implicit equation

$$r_h^{n+1} = \frac{\mu}{1 + a_d^2}. \quad (2.6)$$

For  $n > 1$  this root exists for any value of  $a_d$ . However, it has been shown [27] that the maximum value of  $a_d$  for black holes created by particle collision is  $a_d^{\max} = n/2 + 1$ .

## 2.1 Scalar field equations

In this paper, we study the Hawking emission of scalar fields into the higher-dimensional ‘bulk’ spacetime. Therefore we must first consider the equation of motion for a massless scalar field  $\Phi$  propagating in the bulk, with minimal coupling to the geometry, which satisfies the field equation:

$$\frac{1}{\sqrt{-g}} \partial_\mu (\sqrt{-g} g^{\mu\nu} \partial_\nu \Phi) = 0. \quad (2.7)$$

Here,  $\sqrt{-g}$  is the determinant of the metric,

$$\sqrt{-g} = \Sigma r^n \sin \theta \cos^n \theta \prod_{i=1}^{n-1} \sin^i \theta_i. \quad (2.8)$$

Substituting in (2.7) the factorization ansatz

$$\Phi_\Lambda = e^{-i\omega t} e^{im\psi} R_\Lambda(r) S_\Lambda(\theta) Y_{jn}(\theta_1, \dots, \theta_{n-1}, \phi), \quad (2.9)$$

where  $\Lambda \equiv \{l, m, j, \omega\}$ , yields three coupled second-order equations. The first equation,

$$\sum_{k=1}^{n-1} \frac{1}{\prod_{i=1}^{n-1} \sin^i \theta_i} \partial_{\theta_k} \left[ \left( \prod_{i=1}^{n-1} \sin^i \theta_i \right) \frac{\partial_{\theta_k} Y_{jn}}{\prod_{i>k}^{n-1} \sin^2 \theta_i} \right] + \frac{\partial_{\phi\phi} Y_{jn}}{\prod_{i=1}^{n-1} \sin^2 \theta_i} + j(j+n-1) Y_{jn} = 0, \quad (2.10)$$

defines the *hyperspherical harmonics* on the  $n$ -sphere,  $Y_{jn}$  [28]. The remaining two equations determine the angular  $S_\Lambda(\theta)$  and radial  $R_\Lambda(r)$  mode functions. They are [19]:

$$\frac{1}{\sin \theta \cos^n \theta} \partial_\theta (\sin \theta \cos^n \theta \partial_\theta S_\Lambda) + \left( \omega^2 a^2 \cos^2 \theta - \frac{m^2}{\sin^2 \theta} - \frac{j(j+n-1)}{\cos^2 \theta} + E_\Lambda \right) S_\Lambda = 0, \quad (2.11)$$

and

$$\frac{1}{r^n} \partial_r (r^n \Delta \partial_r R_\Lambda) + \left( \frac{K^2}{\Delta} - \frac{j(j+n-1)a^2}{r^2} - [E_\Lambda + 2am\omega - a^2\omega^2] \right) R_\Lambda = 0, \quad (2.12)$$

where  $K = (r^2 + a^2)\omega - am$ . The angular (2.11) and radial (2.12) equations are coupled through the angular eigenvalue  $E_\Lambda$ , which depends on the spheroidicity parameter  $a\omega$ . There is no known closed analytic form for the eigenvalues, but at least three methods are available for their calculation. First, and simplest,  $E_\Lambda$  may be expressed as a power series in  $a\omega$ . The coefficients of the power series up to 4th order in  $a\omega$  are given in [29]. Alternative numerical methods are Leaver’s method of continued fractions [30], and a numerical matching method, described fully in section 3.1.

Note that the angular equation (2.11) together with the boundary conditions of regularity of the solution at the points  $\theta = 0$  and  $\theta = \pi/2$  constitutes a Sturm-Liouville eigenvalue problem. Orthogonality of the solutions with the appropriate measure follows, and we normalize them so that

$$\int_0^{\pi/2} d\theta \sin \theta \cos^n \theta S_{l'mj\omega} S_{lmj\omega} = \delta_{l'l}. \quad (2.13)$$

Similarly, the hyperspherical harmonics are orthogonal and we normalize them as

$$\int d\phi \prod_{i=1}^{n-1} d\theta_i \prod_{k=1}^{n-1} \sin^k \theta_k Y_{j'n} Y_{jn}^* = \delta_{j'j}. \quad (2.14)$$

## 2.2 Hawking emission

The quantization of the scalar field in the higher-dimensional curved space-time follows through in essentially the same manner as in the 4-D case. We will therefore merely indicate the main steps in the quantization and derivation of the flux formulae and we refer the interested reader to, for example, papers [31, 32, 33] for the 4-D case and to [14] for the  $n = 1$  case.

We define the inner product of two solutions  $\Psi$  and  $\Phi$  of the scalar equation (2.7) in the bulk as

$$\langle \Psi, \Phi \rangle = \frac{i}{2} \int_{\Sigma} d\Sigma^{\mu} \sqrt{-g} (\Phi_{;\mu}^* \Psi - \Psi_{;\mu}^* \Phi), \quad (2.15)$$

where a semicolon denotes the covariant derivative,  $\Sigma$  is a complete Cauchy surface and  $d\Sigma^{\mu}$  is a future-directed normal to  $\Sigma$  (in this section only, the symbol  $\Sigma$  will be used to denote a complete Cauchy surface rather than the function in equation (2.2)). Using the scalar field equation it can be checked that this inner product is independent of the choice of the complete Cauchy surface  $\Sigma$ .

We will follow Myers and Perry [26], and define null coordinates  $u$  and  $v$  as

$$u \equiv t - r_*, \quad v \equiv t + r_*, \quad (2.16)$$

where  $r_*$  is a “tortoise” radial co-ordinate defined as

$$r_* \equiv r + \frac{1}{2\kappa} \log \left( \frac{r - r_h}{r_h} \right), \quad (2.17)$$

and  $\kappa$  is the surface gravity, which is given by [26],

$$\kappa \equiv \frac{(n+1) + (n-1)a_d^2}{2(1+a_d^2)r_h} = \lim_{r \rightarrow r_h} \left[ \frac{\Delta}{2(r_h^2 + a^2)(r - r_h)} \right]. \quad (2.18)$$

The null congruences are tangent to surfaces of constant  $u$  or  $v$  at the horizon ( $r = r_h$ ) and at infinity ( $r \rightarrow \infty$ ), but this is generally not the case for other values of  $r$ . We can also define the Kruskal-like co-ordinates,

$$U \equiv -e^{-u\kappa}, \quad V \equiv e^{v\kappa}. \quad (2.19)$$

We will choose  $\Sigma = \mathcal{J}^- \cup \mathcal{H}^-$  as the Cauchy surface, where  $\mathcal{J}^-$  is the past null infinity given by  $U = -\infty$  and  $\mathcal{H}^-$  is the past horizon given by  $V = 0$ . The surface element in these regions can be calculated,

$$d\Sigma^\mu = \frac{(r_h^2 + a^2)(r - r_h)}{(r^2 + a^2 \cos^2 \theta)U} l^\mu dU d\theta d\psi d\theta_1 \dots d\theta_{n-1} d\phi \quad \text{at } \mathcal{H}^-, \quad (2.20a)$$

$$d\Sigma^\mu = -\frac{1}{2\kappa V} n^\mu dV d\theta d\psi d\theta_1 \dots d\theta_{n-1} d\phi \quad \text{at } \mathcal{J}^-, \quad (2.20b)$$

where  $l$  and  $n$  are two null vector fields,

$$l = l^\mu \frac{\partial}{\partial x^\mu} = \frac{(r^2 + a^2)}{\Delta} \left[ \frac{\partial}{\partial t} + \frac{a}{(r^2 + a^2)} \frac{\partial}{\partial \psi} \right] - \frac{\partial}{\partial r}, \quad (2.21a)$$

$$n = n^\mu \frac{\partial}{\partial x^\mu} = \frac{(r^2 + a^2)}{\Delta} \left[ \frac{\partial}{\partial t} + \frac{a}{(r^2 + a^2)} \frac{\partial}{\partial \psi} \right] + \frac{\partial}{\partial r}. \quad (2.21b)$$

The radial equation (2.12) has singular points at  $r = r_h$  and infinity. We can define two sets of linearly-independent radial solutions (valid for  $n > 0$ ) with the asymptotic behaviours,

$$R_\Lambda^{\text{in}} \sim \begin{cases} (r_d - 1)^{-i\tilde{\omega}/2\kappa}, & r \rightarrow r_+, \\ \frac{1}{r_d^{1+n/2}} (A_\Lambda^{\text{in}} e^{-i\omega_d r_d} + A_\Lambda^{\text{out}} e^{+i\omega_d r_d}), & r \rightarrow +\infty, \end{cases} \quad (2.22a)$$

$$R_\Lambda^{\text{up}} \sim \begin{cases} B_\Lambda^{\text{in}} (r_d - 1)^{-i\tilde{\omega}/2\kappa} + B_\Lambda^{\text{out}} (r_d - 1)^{+i\tilde{\omega}/2\kappa}, & r \rightarrow r_+, \\ \frac{1}{r_d^{1+n/2}} e^{+i\omega_d r_d}, & r \rightarrow +\infty, \end{cases} \quad (2.22b)$$

where  $A_\Lambda^{\text{in}}$ ,  $A_\Lambda^{\text{out}}$ ,  $B_\Lambda^{\text{in}}$  and  $B_\Lambda^{\text{out}}$  are complex constants,  $\tilde{\omega} \equiv \omega - m\Omega_h$  and  $\Omega_h = a/(r_h^2 + a^2)$  is the angular speed of the horizon. We define the ‘in’ solutions for  $\omega > 0$  and the ‘up’ solutions for  $\tilde{\omega} > 0$ .

The field mode solutions  $\Phi_\Lambda^{\text{in/up}}$  constructed via equation (2.9) from equations (2.22) satisfy the normalization conditions

$$\langle \Phi_\Lambda^{\bullet*}, \Phi_{\Lambda'}^{\bullet'} \rangle = 0, \quad \langle \Phi_\Lambda^{\bullet}, \Phi_{\Lambda'}^{\bullet'} \rangle = \delta_{\Lambda\Lambda'} \delta_{\bullet\bullet'}, \quad (2.23)$$

after an appropriate normalization factor is included, where symbols  $\bullet$  and  $\bullet'$  denote either the ‘in’ or the ‘up’ solutions. The normalization factors can be calculated using the surface elements (2.20) and, when included, the field modes are explicitly given by

$$\Phi_\Lambda^{\text{in}} = \frac{1}{2\pi\sqrt{\omega} r_h^{n/2+1} |A_\Lambda^{\text{in}}|} e^{-i\omega t} e^{im\psi} R_\Lambda^{\text{in}}(r) S_\Lambda(\theta) Y_{jn}(\theta_1, \dots, \theta_{n-1}, \phi), \quad (2.24)$$

$$\Phi_\Lambda^{\text{up}} = \frac{1}{2\pi\sqrt{K(r_h)} r_h^{n/2} |B_\Lambda^{\text{out}}|} e^{-i\omega t} e^{im\psi} R_\Lambda^{\text{up}}(r) S_\Lambda(\theta) Y_{jn}(\theta_1, \dots, \theta_{n-1}, \phi), \quad (2.25)$$

where the orthogonality relations (2.13) and (2.14) have been used.

The field mode solutions ‘in’ and ‘up’ form a complete set of orthonormal solutions to the scalar equation (2.7) in the outer region of the space-time. A general solution of the scalar equation can therefore be written as a linear combination of this basis

$$\Phi(x) = \sum_{\Lambda} \sum_{\bullet=\text{in,up}} \left[ a_\Lambda \Phi_\Lambda^{\bullet}(x) + a_\Lambda^* \Phi_\Lambda^{\bullet*}(x) \right], \quad (2.26)$$

where the integration over the frequency is for  $\omega > 0$  for the ‘in’ modes and for  $\tilde{\omega} > 0$  for the ‘up’ modes. Promoting the fields and the Fourier coefficients  $a_\Lambda$  to operators  $\hat{a}_\Lambda$ , using the normalization conditions (2.23) and imposing the standard canonical commutation relations for the field and its canonical momenta leads to the commutation relations

$$[\hat{a}_\Lambda^\bullet, \hat{a}_{\Lambda'}^{\bullet'}] = [\hat{a}_\Lambda^{\bullet\dagger}, \hat{a}_{\Lambda'}^{\bullet'\dagger}] = 0, \quad [\hat{a}_\Lambda^\bullet, \hat{a}_{\Lambda'}^{\bullet'\dagger}] = \delta_{\Lambda\Lambda'} \delta_{\bullet\bullet'}. \quad (2.27)$$

In the eternal version of the space-time (i.e. in the full analytic extension of the Myers-Perry metric) we can construct from the field modes  $\Phi_\Lambda^{\text{in/up}}$  a complete orthonormal basis of modes which are positive-frequency with respect to both the affine parameter  $U$  on the past horizon  $\mathcal{H}^-$  and the affine parameter  $t$  on past null infinity  $\mathcal{J}^-$ . The past Unruh state  $|U^-\rangle$  is defined [31, 34] as the quantum state which is annihilated by the Fourier coefficients – as operators – of this basis of modes. This state models an evaporating black hole and is therefore the relevant one for computing the Hawking emission.

The stress-energy tensor for a minimally coupled scalar field is given by

$$T_{\mu\nu}[\Phi, \Phi^*] = \frac{1}{2} [\Phi_{;\mu} \Phi_{;\nu}^* + \Phi_{;\nu} \Phi_{;\mu}^*] - \frac{1}{2} g_{\mu\nu} \Phi^{;\alpha} \Phi_{;\alpha}^*. \quad (2.28)$$

It can be proven [31, 32] that the expectation value of the stress-energy tensor operator when the scalar field is in the past Unruh state is given by

$$\langle U^- | \hat{T}_{\mu\nu} | U^- \rangle = \sum_{l,j,m} \left( \int_0^\infty d\tilde{\omega} \coth\left(\frac{\tilde{\omega}}{2T_H}\right) T_{\mu\nu}[\Phi_\Lambda^{\text{up}}, \Phi_\Lambda^{\text{up}*}] + \int_0^\infty d\omega T_{\mu\nu}[\Phi_\Lambda^{\text{in}}, \Phi_\Lambda^{\text{in}*}] \right) \quad (2.29)$$

with the Hawking temperature

$$T_H = \frac{\kappa}{2\pi}. \quad (2.30)$$

It is well-known that the expectation value of the stress-energy tensor is generally divergent and it must be renormalized appropriately. One method of renormalization is the technique of covariant geodesic point separation. In this approach, the pair of fields appearing in each quadratic term in the stress-energy tensor (2.28) are evaluated at separate points,  $x$  and  $x'$ . This defines a bi-tensor  $T_{\mu\nu}(x, x')$ . The expectation value of this bi-tensor is found for the desired quantum state, and certain purely geometric terms  $T_{\mu\nu}^{\text{div}}(x, x')$  are subtracted from it. Finally, the two points are moved together again, i.e. the coincidence limit  $x' \rightarrow x$  is taken. In 4-D, Christensen [35, 36] calculated the geometric subtraction terms using the Schwinger-DeWitt expansion [37, 38] for the Hadamard elementary function. The Schwinger-DeWitt expansion for the non-rotating, higher-dimensional case is given in [39]. In principle this could be used to compute the geometric subtraction terms in higher dimensions, following [35, 36], but fortunately we do not require their precise form in our analysis.

In [33] it was shown that those components of the unrenormalized expectation value of the stress-energy tensor with one index either  $t$  or  $\psi$  and the other index  $r$  (as in (2.31) below) are not divergent and so do not require renormalization. The proof is based on two properties. Firstly, we use the symmetry of the metric under  $(t, \psi) \rightarrow (-t, -\psi)$ . Secondly,



each of the geometric subtraction terms contains an even number of covariant derivatives  $\sigma^\mu$  of the biscalar of geodetic interval [40] after an average is taken over a separation in the  $\sigma^\mu$  and  $-\sigma^\mu$  directions. By choosing a point-splitting in the radial direction, these two properties then ensure that the geometric subtraction terms  $T_{tr}^{\text{div}}(x, x')$  and  $T_{r\psi}^{\text{div}}(x, x')$  vanish (see [33] for the full argument). Even without explicitly computing the geometric subtraction terms, it can be shown that these two properties remain true in higher dimensions, so that the argument of [33] follows through, and we have  $T_{tr}^{\text{div}}(x, x') = T_{r\psi}^{\text{div}}(x, x') = 0$  independent of  $n$ , the number of extra dimensions.

Having established that the  $tr$  and  $\psi r$  components do not require renormalization, the fluxes of energy and angular momentum are given by

$$\begin{aligned}\frac{dE}{dt} &= \Delta \int_S d\Omega_{n+2} \left\langle U^- \left| \hat{T}_{tr} \right| U^- \right\rangle, \\ \frac{dJ}{dt} &= \Delta \int_S d\Omega_{n+2} \left\langle U^- \left| \hat{T}_r^\psi \right| U^- \right\rangle,\end{aligned}\tag{2.31}$$

where  $S$  is any surface of constant  $t$  and  $r$ . The total rate of energy emission of massless scalars into the bulk is found by taking a sum over all angular modes. Taking for the surface  $S$  in (2.31) a  $(2+n)$ -sphere boundary at infinity and using equations (2.29) and (2.22), it can be shown [14, 19] that

$$\frac{d^2 E}{dt d\omega} = \frac{1}{2\pi} \sum_{l,j,m} \frac{\omega}{\exp(\tilde{\omega}/T_H) - 1} N_j \mathcal{T}_\Lambda \tag{2.32}$$

and the emission rate of angular momentum into the bulk is given by

$$\frac{d^2 J}{dt d\omega} = \frac{1}{2\pi} \sum_{l,j,m} \frac{m}{\exp(\tilde{\omega}/T_H) - 1} N_j \mathcal{T}_\Lambda. \tag{2.33}$$

Here,  $\mathcal{T}_\Lambda$  is the energy-dependent *transmission factor* (also known as ‘greybody factor’) and is given by the ratio of the ingoing and outgoing fluxes,

$$\mathcal{T}_\Lambda = 1 - \left| \frac{A_\Lambda^{\text{out}}}{A_\Lambda^{\text{in}}} \right|^2. \tag{2.34}$$

In addition,  $N_j$  is a degeneracy factor (given in equation (11) of [28]) which accounts for the multiplicity of modes in the bulk,

$$N_j = \frac{(2j+n-1)(j+n-2)!}{j!(n-1)!}. \tag{2.35}$$

All parts of equation (2.32) can be determined analytically, except for the transmission factors  $\mathcal{T}_\Lambda$ . Qualitatively, the transmission factor is a dimensionless measure of the proportion of a given mode that can escape from the black hole horizon to reach infinity. Hence,  $\mathcal{T}_\Lambda = 1$  corresponds to ‘total’ emission, and  $\mathcal{T}_\Lambda = 0$  to ‘total’ back-reflection of Hawking radiation. The transmission factors in turn determine the shape and magnitude of the power spectrum. Approximate expressions for  $\mathcal{T}_\Lambda$  were recently presented in the literature [19]. In this study, we determine them numerically by solving the radial equation (2.12). Our numerical method is outlined in section 3.2.

### 3. Numerical methods

In this section we briefly describe the numerical methods we employ for computing the angular eigenvalues and the transmission factors.

#### 3.1 Angular eigenvalues

The allowed values of the angular momentum quantum numbers  $l$ ,  $j$  and  $m$  are restricted [29]. The azimuthal number  $m$  can take any integer value, and  $l$  and  $j$  are positive or zero integers, such that

$$l \geq j + |m| \quad \text{and} \quad l - j - |m| = 2k, \quad \text{where } k \in \{0, \mathbb{Z}^+\}. \quad (3.1)$$

The second equation in (3.1) implies that only even [odd] values of  $l$  are allowed when  $(j + |m|)$  is even [odd]. Note that the angular equation (2.11) has two regular singular points at  $\theta = 0$  and  $\theta = \pi$ , just like the 4-D spin-weighted spheroidal equation (equation (2.11) with  $j = n = 0$ ), plus an extra regular singular point at  $\theta = \pi/2$ , which is a non-singular point in the 4-D case. The presence of this extra regular singular point means that half the regular solutions in the 4-D case will now, for  $n > 0$ , become irregular. This is the reason why the angular momentum quantum number  $l$  is forced to have the same parity as  $j + |m|$  (as opposed to being allowed to be any non-negative integer in the 4-D case). Note also that the whole of the physical region in the bulk is covered by the regime  $\theta \in [0, \pi/2]$ . However, when restricting ourselves to the brane (by taking  $\theta_1 = 0$ ), the whole physical region is covered by extending the regime to  $\theta \in [0, \pi]$  (in the same way as when vertically slicing a 2-sphere into two halves we must extend the regime of the polar angle from  $\theta \in [0, \pi]$  to  $\theta \in [0, 2\pi]$  in order to cover the full circle).

The numerical method we used for solving the angular equation in the bulk, equation (2.11), is essentially the same – with the obvious modifications – as the shooting method for the 4-D case as described in detail in [41], to which we refer the interested reader. We require power series expansions around the two integration end-points  $\theta = 0$  and  $\theta = \pi/2$ . Near the end-point  $\theta = \pi/2$  we used the power series expansion given in equation (3.4) of [29]. Near the other end-point  $\theta = 0$  (or  $\theta = \pi$ , by symmetry) we insert the expansion

$$S_\Lambda = (\sin \theta)^{|m|} (\cos \theta)^j \sum_{p=0}^{\infty} a_p (1 \pm \cos \theta)^p \quad (3.2)$$

into equation (2.11) and obtain the recursion relation:

$$a_{p+1} = \frac{1}{\alpha_p} \{ \beta_p a_p + \gamma_p a_{p-1} + \delta_p a_{p-2} + \epsilon_p a_{p-3} \}, \quad (3.3)$$

where

$$\begin{aligned}
\alpha_p &= 2(p+1)(p+|m|+1), \\
\beta_p &= [3(p-1) + 2(n+2j) + 4(|m|+1)]p - (a\omega)^2 - E_\Lambda + j(j+n+1) \\
&\quad + |m|(n+|m|+2j+1), \\
\gamma_p &= 3(a\omega)^2 - p(p+n+2j+2|m|-1) + n + E_\Lambda - j(j+n-1) \\
&\quad - |m|(n+|m|+2j-1), \\
\delta_p &= -3(a\omega)^2, \\
\epsilon_p &= (a\omega)^2.
\end{aligned} \tag{3.4}$$

It is easy to check that for  $n = j = 0$  this recursion relation coincides with the corresponding one in the 4-D case (see, e.g., equations (2.5)–(2.8) with spin  $s = 0$  in [29]).

The eigenvalues  $E_\Lambda$  in the 4-D case become degenerate for large  $a\omega$  [41]. Fortunately, this degeneracy does not occur in the bulk case [29]. Therefore, the integration of the angular equation with our technique is more amenable in the bulk than in 4-D for large  $a\omega$ .

### 3.2 Transmission factors

To compute the transmission factors  $\mathcal{T}_\Lambda$  we solved the radial equation (2.12) numerically. We started with the ingoing solution close to the horizon and integrated out to large  $r_d$ . Here, we matched the numerical solution onto the asymptotic form (2.22a) to determine  $A_\Lambda^{\text{in}}$  and  $A_\Lambda^{\text{out}}$  and hence, via (2.34),  $\mathcal{T}_\Lambda$ . Typically, we integrated from  $r_d = 1.001$  to a matching point at  $r_d = 100$ .

The solution close to the horizon may be found using the method of Frobenius. The radial equation (2.12) may be rewritten

$$\frac{d^2 R_\Lambda}{d\eta^2} = \frac{A(\eta)}{\eta} \frac{dR_\Lambda}{d\eta} + \frac{B(\eta)}{\eta^2} R_\Lambda, \tag{3.5}$$

where  $\eta = r/r_h - 1$ . Here,  $A(\eta)$  and  $B(\eta)$  are functions with Maclaurin series expansions,

$$A(\eta) = \sum_{j=0} A_j \eta^j, \quad B(\eta) = \sum_{j=0} B_j \eta^j. \tag{3.6}$$

The coefficients  $A_j$  and  $B_j$  are easily determined using a mathematical software package such as Maple. Near the horizon, the radial solution may be expressed as a power series in  $\eta$ ,

$$R_\Lambda(\eta) = \eta^s \sum_{j=0} R_j \eta^j. \tag{3.7}$$

The index  $s$  satisfies the indicial equation  $s(s-1) - sA_0 - B_0 = 0$ , which has solutions  $s = \pm i\tilde{\omega}/(2\kappa)$ . The negative root is the correct choice for an ingoing solution. The coefficients  $R_j$  are determined from the recurrence relation

$$[(s+j)(s+j-1) - (s+j)A_0 - B_0] R_j = \sum_{k=1}^j [(s+j-k)A_k + B_k] R_{j-k}. \tag{3.8}$$

We used this method to compute expansion coefficients up to  $R_5$ .

The ingoing and outgoing solutions in the large- $r_d$  limit may be found by a similar method. First we make the substitution

$$R_\Lambda(r) = \frac{e^{\pm i\omega_d r_d}}{r_d^{1+n/2}} X_\Lambda(r), \quad n \in \mathbb{Z}^+. \quad (3.9)$$

The positive (negative) sign in the exponent gives the outgoing (ingoing) solution. This substitution leads to a differential equation which can be written

$$\frac{d^2 X_\Lambda}{dz^2} = \left( \frac{\pm 2i\omega_d}{z^2} + \frac{C(z)}{z} \right) \frac{dX_\Lambda}{dz} + \frac{D(z)}{z^2} X_\Lambda \quad (3.10)$$

where  $z = 1/r_d$ . Again,  $C(z)$  and  $D(z)$  have Maclaurin series expansions which can be easily found with a symbolic algebra package. The radial function  $X_\Lambda(z)$  also has a Maclaurin series expansion,  $X_\Lambda(z) = \sum_{j=0} X_j z^j$ , with coefficients  $X_j$  determined by the recurrence relation

$$\pm 2i\omega_d(j+1)X_{j+1} = j(j-1)X_j - \sum_{k=0}^j ((j-k)C_k + D_k)X_{j-k}. \quad (3.11)$$

We computed coefficients  $X_j$  up to tenth order. Note that the ingoing solution is simply the complex conjugate of the outgoing solution.

## 4. Results

In this section we present numerical results for the emission of scalars by a rotating higher-dimensional black hole. Our objective is to compare the relative magnitudes of emission into the bulk and on to the brane. First, we begin with a review of the results for the Schwarzschild (non-rotating) phase [12]. Next, we examine the effect of black hole rotation upon the transmission factors and emission spectra. In its rotating phase, the black hole is shedding both mass and angular momentum; we determine the loss rates for both quantities. We conclude by presenting bulk-to-brane emission ratios for a range of values of  $a_d$  and  $n$ .

### 4.1 Non-rotating black holes ( $a_d = 0$ )

A detailed study of scalar brane and bulk emission in the non-rotating phase was presented in [12]. Here we review some key results of that work.

Figure 1 shows the power spectrum on the brane (left) and in the bulk (right) for  $n = 1, 2 \dots 6$ . The total emission rate, or power, is equivalent to the area under the curves. The total emission depends strongly on the number of bulk dimensions,  $n$ . For all  $n$ , the total power emitted on the brane exceeds that emitted into the bulk (note the  $y$ -scales in figure 1). This is despite the fact that particles emitted into the bulk are, on average, more energetic than those emitted on the brane.

Table 1 shows the total power (in units of  $1/r_h^2$ ) for  $n = 1, 2 \dots 6$ . The total power increases monotonically with  $n$ . The proportion of the total power that is emitted into the

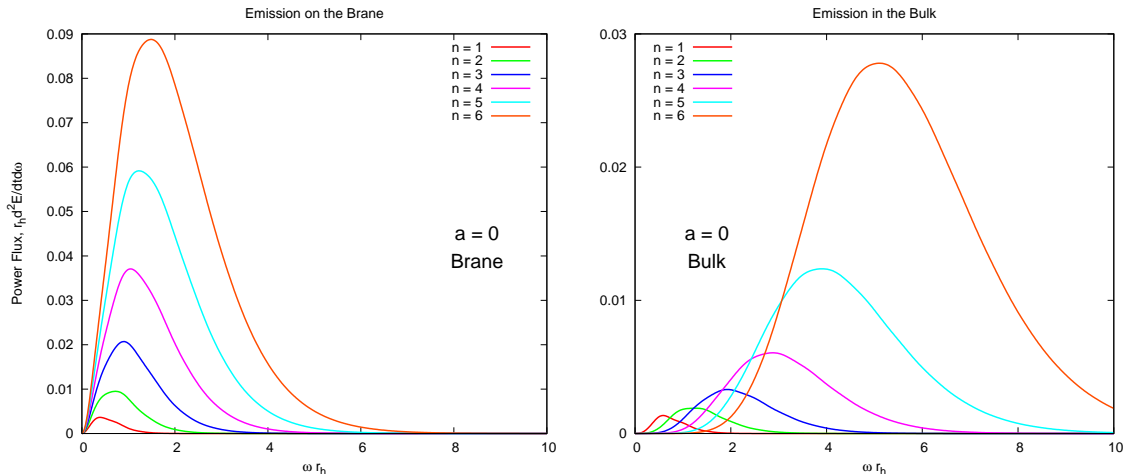


**Figure 1:** *Brane and bulk emission from a non-rotating higher-dimensional black hole.* The left plot shows the power emitted on the brane, for various numbers of space-time dimensions ( $n = 1, 2 \dots 6$ ). The right plot shows the power emitted into the bulk. Note the factor of 3 difference in the scales on the  $y$ -axis.

	$n = 1$	$n = 2$	$n = 3$	$n = 4$	$n = 5$	$n = 6$
Total Power, $r_h^2 dE/dt$	0.00371	0.0134	0.0362	0.0823	0.170	0.339
% in bulk	28.3%	19.9%	17.9%	19.6%	24.8%	34.0%

**Table 1:** *Proportion of scalar power emitted into the bulk by a non-rotating black hole.* These quantities were calculated by numerically integrating the power spectra up to a frequency cutoff of  $\omega r_h = 10$ . The values are in good agreement with earlier studies [12].

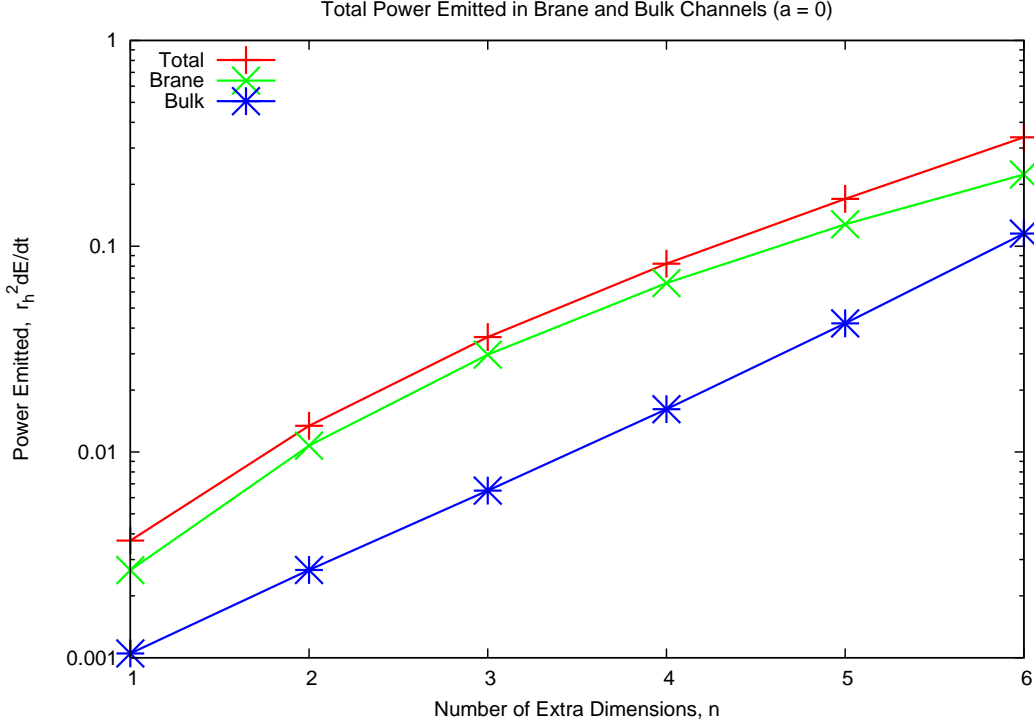
bulk (i.e. the ‘missing’ energy fraction) decreases for  $n$  from 1 to 3, but increases again for  $n > 3$ .

Figure 2 shows how the proportion of energy lost in the bulk depends on  $n$ . The total power emitted in the bulk appears to obey a power law relationship,  $r_h^2 \frac{dE}{dt} \sim A\sigma^n$ , where  $A \sim 0.0004$  and  $\sigma \sim 2.54$ . The power emitted on the brane increases less rapidly with  $n$ . Hence the proportion of total energy lost in the bulk decreases up to  $n = 3$ , but increases for  $n > 3$ .

The key question that we seek to address in the next section is: how does the proportion of energy lost into the bulk change when the black hole is rotating? In other words, is the standard claim [22] that *black holes radiate mainly on the brane* still correct in the spin-down phase of black hole evolution?

## 4.2 Rotating black holes, $a_d > 0$

Here we consider a black hole rotating in the  $\theta = \pi/2$  plane on the brane. Introducing a single plane of rotation has many consequences: it modifies the angular eigenvalues, the transmission factors, and the form of the mode sum. Rotation breaks the azimuthal degeneracy, so that modes of different  $m$  contribute different amounts of power.



**Figure 2:** Total power (in scalar particles) emitted by a non-rotating black hole. The blue line shows the power emitted in the bulk, and the green line shows the power emitted on to the brane, for various  $n$  (the number of extra dimensions). Note the logarithmic scale on the  $y$ -axis.

Previous studies [15, 18] have shown that, overall, rotation enhances the emission on the brane. Higher angular momentum modes become increasingly important, and the black hole emits particles at higher energies. The superradiant effect increases the emission from the co-rotating modes, particularly for low  $n$ . For fast-rotating black holes, the  $m = l$  modes dominate the emission. This leads to an oscillatory power spectrum, and a rapid loss of black hole angular momentum.

#### 4.2.1 Transmission factors

Let us begin by considering the transmission factors  $\mathcal{T}_\Lambda$ , defined by equation (2.34). An analytic expression for the transmission factor was derived in [19] under the assumption that both the energy  $\omega_d$  and angular momentum  $a_d$  parameters are much lower than unity. For the indicative case of the  $l = j = m = 0$  mode, the dominant behaviour, as  $\omega \rightarrow 0$ , was also computed and found to be given by the expression

$$\mathcal{T}_{000\omega} \approx \frac{4\pi(1 + a_d^2)^2(\omega r_h)^{n+2}}{A_* 2^n(n+1)\Gamma^2(\frac{n+1}{2})(2 - D_*)}, \quad (4.1)$$

where  $A_* = (n+1) + (n-1)a_d^2$  and  $D_* = 1 - 4a_d^2/A_*^2$ . In figure 3, we compare the approximation of equation (4.1) with our numerically-determined transmission coefficients. We find good agreement in the regime  $\mathcal{T}_\Lambda \lesssim 0.1$ . It is clear that the effect of rotation is to shift the  $l = j = m = 0$  transmission curve to lower energies.

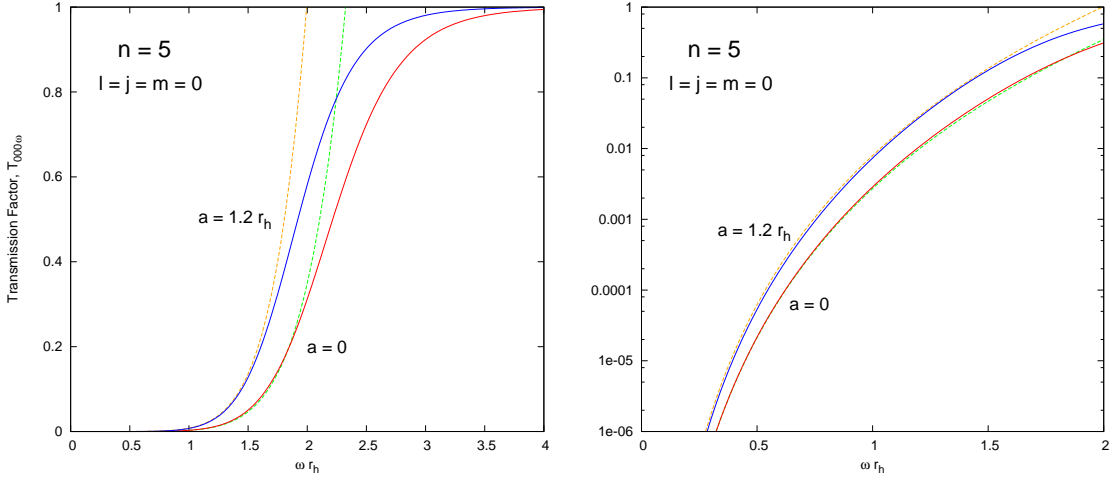
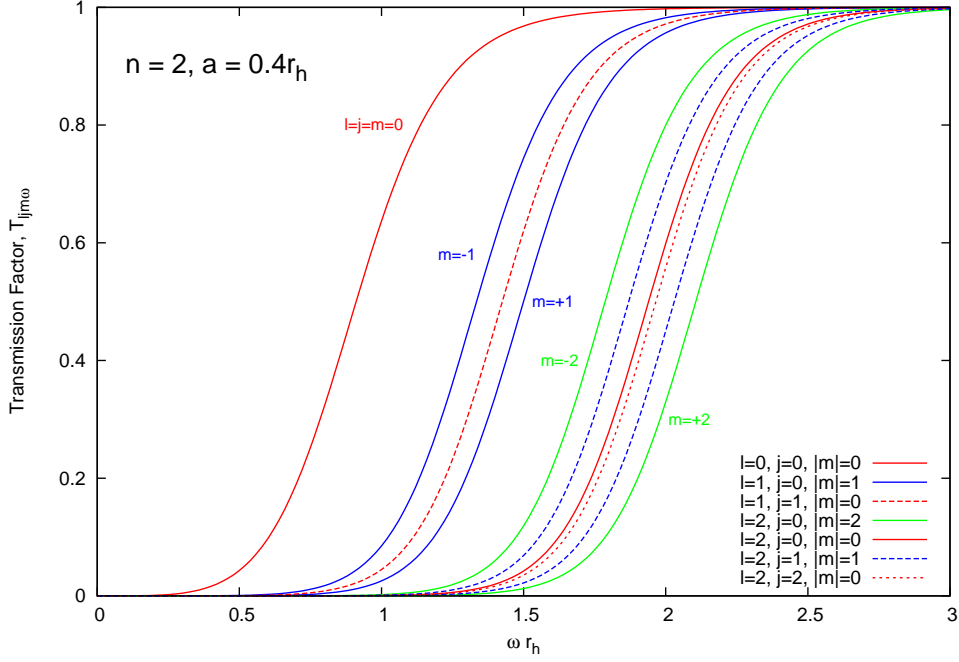


**Figure 3:** Transmission factor of the  $l = j = 0$  mode for  $n = 5$ , for  $a_d = 0.0$  and  $a_d = 1.2$ . This plot compares the approximation [19] (dotted line) given in equation (4.1) with our exact numerical results (solid line). The right plot shows the same data, but with a logarithmic scale on the  $y$ -axis.

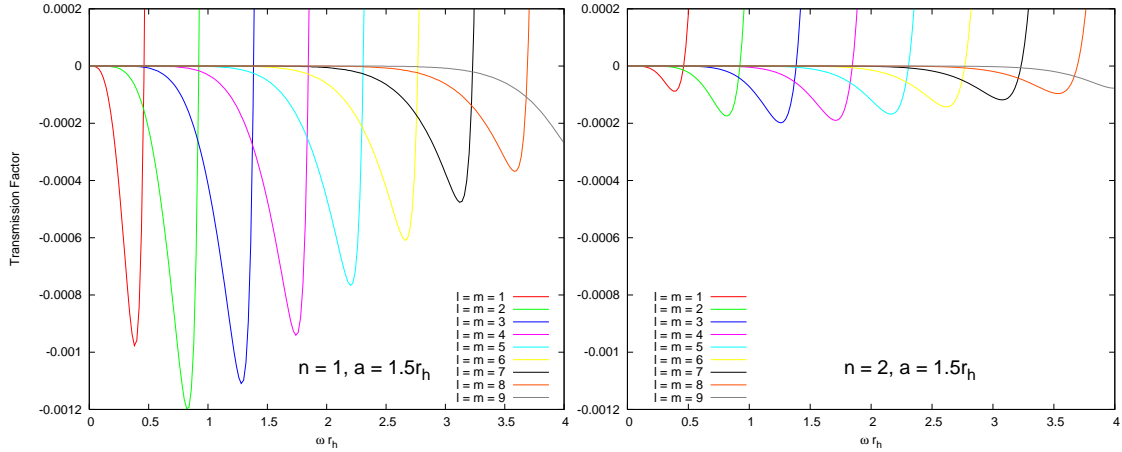
To compute the total cross section, it is not sufficient to consider only the  $l = j = m = 0$  modes. We must compute a sum over all angular modes. The modes are labelled by three integers:  $l$ , the total angular momentum;  $m$ , the angular momentum in the plane of rotation; and  $j$ , the angular momentum in the bulk. These integers satisfy the condition (3.1). If the black hole is rotating then we must compute transmission factors for each valid combination of  $l$ ,  $j$  and  $m$ . In practice, we will truncate the mode sum at some suitable  $l = l_{\text{max}}$ . Unsurprisingly, the multiplicity of modes in the bulk is greater than the multiplicity of modes on the brane. For example, the number of non-degenerate modes  $N(L)$  in the range  $0 \leq l \leq L$  is  $N_{\text{brane}}(L) = (L + 1)^2$  on the brane, but is  $N_{\text{bulk}}(L) = L(L^2 - 1)/6$  in the bulk. The computation time increases commensurately with the number of modes considered.

Figure 4 shows the transmission coefficients for the first few modes, for the particular case of a slowly-rotating 6D hole ( $a_d = 0.4$ ). A hierarchy of effects is clear. The modes are split firstly on  $l$ , secondly on  $m$  and finally on  $j$ . The azimuthal splitting on  $m$  increases in magnitude with rotation parameter  $a_d$ .

In the frequency regime  $\omega < m\Omega_h$ , the superradiance effect causes the transmission coefficient to become negative. Nonetheless, the emitted power is positive, since the denominator of equation (2.32) is also negative in this regime. Superradiance is most significant for the  $m = l$ ,  $j = 0$  modes (i.e. the maximally-corotating modes). Figure 5 shows how superradiance affects the  $m = l$  transmission factors of fast-rotating 5D (left) and 6D (right) black holes. It is clear that superradiance is most significant at low  $n$ . In particular, for  $n = 1$ , superradiance has a significant effect on the shape of the power spectra, as we see in the next section.



**Figure 4:** Transmission factors for the first few modes,  $l = 0, 1$  &  $2$ . The plot shows transmission factors for a 6D black hole rotating at  $a_d = 0.4$ . The three sets of lines correspond to  $l = 0$  (left),  $l = 1$  (middle) and  $l = 2$  (right). For each  $l$ , there is a multiplet of  $(l + 1)(l + 2)/2$  modes. The modes in each multiplet are split by  $m$  and, to a lesser extent, by  $j$ .



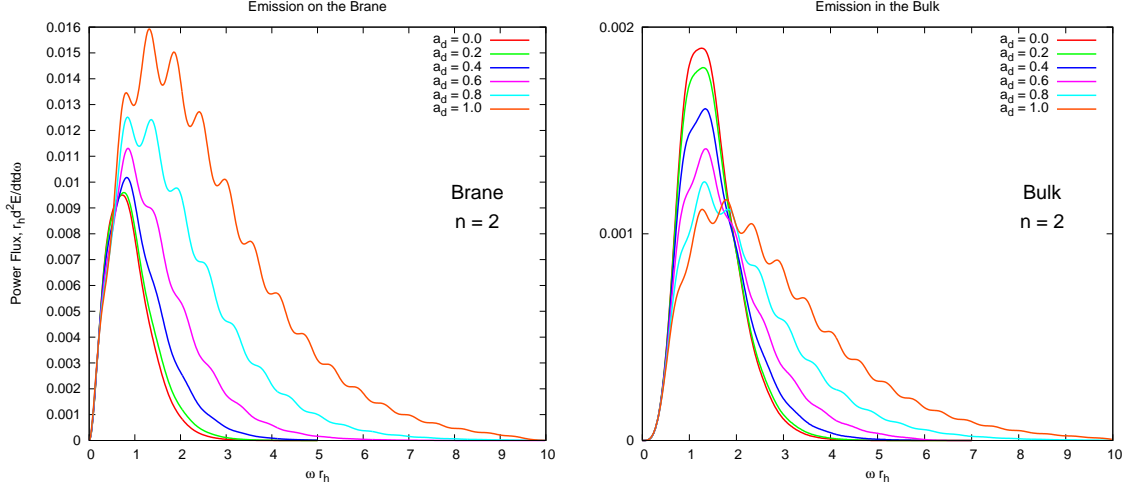
**Figure 5:** Transmission factors for the maximally-rotating  $m = l$  modes of a fast-rotating ( $a_d = 1.5$ ) black hole. The left plot shows transmission factors for a 5D ( $n = 1$ ) black hole, and the right plot shows the same modes for a 6D ( $n = 2$ ) black hole. The transmission factors are negative for  $\omega < m\Omega_h$  due to the superradiance effect.

#### 4.2.2 Power spectra

Let us now consider the effect of rotation on the shape and magnitude of the spectra of



scalar radiation emitted in both the bulk and the brane. As we saw in the previous section, the shape and magnitude of the emission spectrum strongly depends on the number of extra dimensions,  $n$ . Let us examine two cases in detail,  $n = 2$  and  $n = 6$ .



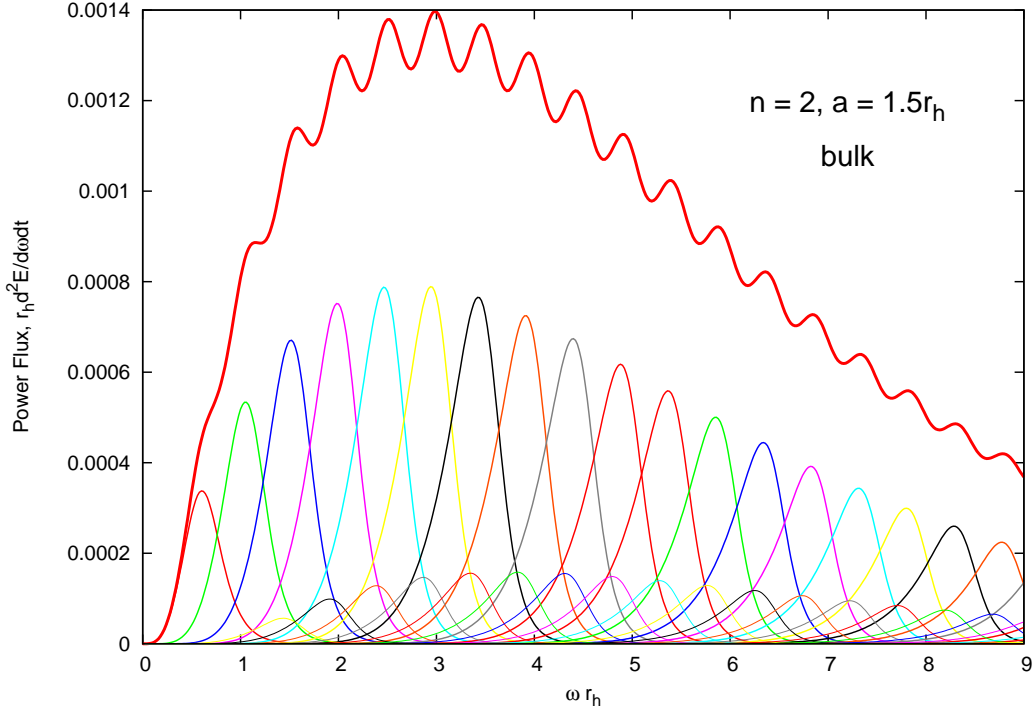
**Figure 6:** *Brane and bulk emission from a 6D rotating black hole.* The left and right plots show the power emitted on the brane and in the bulk, respectively. Black hole rotation increases the proportion of the total flux that is emitted on the brane. Note the order-of-magnitude difference in the scales on the  $y$ -axis.

Figure 6 shows how rotation changes the emission spectrum of a 6D ( $n = 2$ ) black hole. The left panel shows emission on the brane, and the right panel shows emission in the bulk. From the left panel, it can be seen that the total emission on the brane (the area under the curve) increases monotonically with the rotation parameter  $a_d$ . In the bulk, the situation is more complicated. A slowly-rotating black hole actually emits less power into the bulk than a non-rotating hole. However, above  $a_d \sim 0.4$ , the total emission increases with  $a_d$ . The total powers for the curves shown in figure 6 are given in table 2. The reduction in bulk emission is due to the fact that the Hawking temperature (2.30) decreases monotonically with  $a_d$ . Thus, a rotating black hole is cooler than a non-rotating hole. On the brane, the reduction in  $T_H$  is more than outweighed by the fact that rotation changes the transmission factors, and enhances emission in the higher angular modes. In the bulk, this is not necessarily the case, particularly at low  $a_d$ .

	$a_d = 0.0$	$a_d = 0.2$	$a_d = 0.4$	$a_d = 0.6$	$a_d = 0.8$	$a_d = 1.0$
Bulk Power	0.00267	0.00262	0.00256	0.00266	0.00308	0.00391
Brane Power	0.01074	0.01148	0.01414	0.02003	0.03132	0.05142
% in Bulk	19.9%	18.6%	15.3%	11.7%	9.0%	7.1%

**Table 2:** *Proportion of scalar power emitted into the bulk by a 6D rotating black hole.* These figures were calculated by numerically integrating the power spectra, up to a cutoff of  $\omega r_h = 10$ . The power (mass loss rate) is given in units of  $1/r_h^2$ .

In the non-rotating case, emission is primarily in the  $l = 0$  and  $l = 1$  modes. However, rotation enhances the emission from higher angular modes. The oscillatory pattern in the emission spectra at higher  $a_d$  is due to the increasing importance of the superradiant  $m = l$ ,  $j = 0$  modes. This is seen clearly in figure 7, which shows the contribution of the  $m = l$  and  $m = l - 1$  modes to the overall power spectrum.



**Figure 7:** Emission from a 6D black hole at  $a_d = 1.5$ . The plot shows that the majority of the emission comes from the maximally-corotating modes ( $m = l$ ). The  $m = l - 1$  modes are also plotted.

Next, let us consider emission from a 10D ( $n = 6$ ) rotating black hole. Figure 8 compares the power spectra on the brane (left panel) and in the bulk (right panel), at  $a_d = 0.0$  (red),  $a_d = 0.5$  (green) and  $a_d = 1.0$  (blue). It is immediately clear that rotation enhances emission on the brane significantly, but has a lesser effect on emission in the bulk. A large number of angular modes contribute to the total power for  $n = 6$ . Figure 9 compares the relative magnitudes of the  $m = l$ ,  $m = l - 1 \dots, m = l - 5$  modes, at  $a_d = 1.5$ , for  $l = 0, 1, \dots, 26$ . Note that a sum over  $j$  was taken where multiple modes exist with the same  $l$  and  $m$ . With six bulk dimensions, the degeneracy factor  $N_j$  (2.35) appearing in the mode sum is potentially very large. This enhances the contribution from the higher  $j$  modes. The degeneracy factors increase in the sequence  $1, n + 1, n(n + 3)/2, (n + 5)(n + 1)n/6, \dots$  for  $j = 0, 1, 2, 3, \dots$ ; i.e.  $1, 7, 18, 77, \dots$  for  $n = 6$ . Modes close to  $m = 0$  have a much higher degeneracy than modes near  $m = l$ . For each  $m$ , the most significant contributions arise from the  $j = l - m$  modes.

Figure 10 compares the emission on the brane (left) and in the bulk (right) at  $a_d = 1.0$ ,

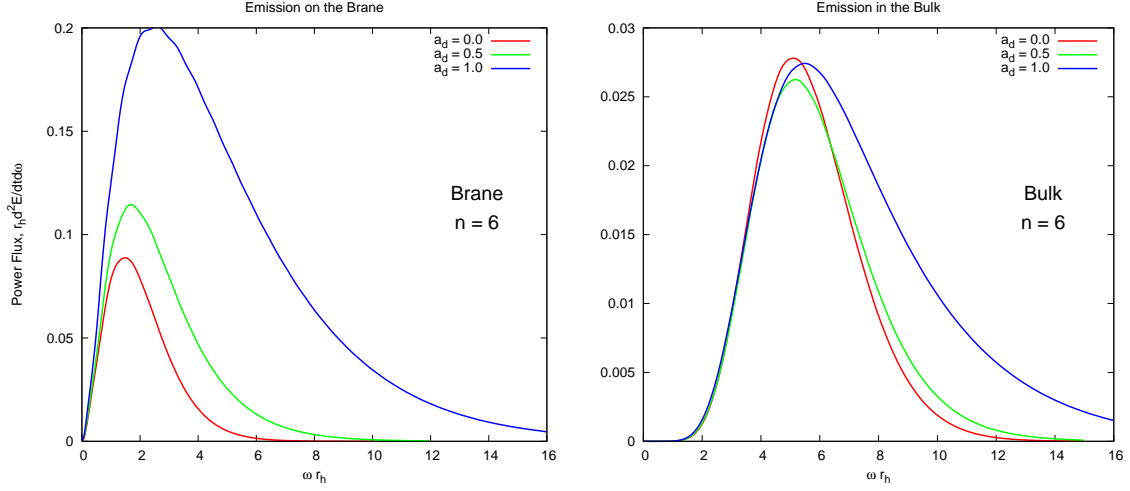


**Figure 8:** *Brane and bulk emission from a 10D rotating black hole.* The left and right plots show the power emitted on the brane and in the bulk, respectively. Black hole rotation increases the proportion of the total power that is emitted on the brane. Note the order-of-magnitude difference in the scales on the  $y$ -axis.

for a range of  $n = 1, 2 \dots 6$ . Note that the scale on the  $y$ -axes differs by a factor of  $\sim 7$ . Comparing these spectra with the non-rotating spectra of figure 1, it is clear that rotation has reduced the proportion of the overall emission which enters the bulk. Table 3 lists the fraction of power lost in the bulk, for a range of scenarios. This data is plotted in figure 11, which shows the % of scalar power in the bulk for  $a_d = 0 \dots 1$  and  $n = 1, 2, \dots 6$ .

	$a_d = 0.0$		$a_d = 0.5$		$a_d = 1.0$	
$n = 1$	28.3%	0.00371	20.9%	0.00449	12.5%	0.01154
$n = 2$	19.9%	0.0134	13.5%	0.01953	7.1%	0.05533
$n = 3$	17.9%	0.0362	11.8%	0.05497	6.2%	0.1646
$n = 4$	19.6%	0.0823	13.0%	0.1275	6.8%	0.3808
$n = 5$	24.8%	0.170	16.7%	0.2609	9.1%	0.7709
$n = 6$	34.0%	0.339	24.0%	0.5041	14.7%	1.3832

**Table 3:** *Proportion of total power emitted into the bulk.* This table gives the percentage of the total power (i.e. the combined bulk and brane mass loss rate, in units of  $1/r_h^2$ ) that is emitted into the bulk, for a range of dimensionalities  $n$ , and angular momenta  $a_d$ . The total powers were calculated by numerically integrating the power spectra up to cutoffs of  $\omega r_h = 10, 12$  and  $16$ , for  $a_d = 0.0, 0.5$  and  $1.0$ , respectively.

Finally, let us briefly consider very fast rotation,  $a_d > 1$ . As we have seen, a large number of modes are excited by a fast-rotating black hole. For instance, figure 9 shows that modes up to  $l \sim 30$  contribute to the emission spectrum of a 10D hole at  $a_d = 1.5$ , and that the power spectrum is significant at  $\omega r_h \sim 15$  and beyond. Such spectra may give a misleading impression, since the black hole cannot emit a pair of particles which are more

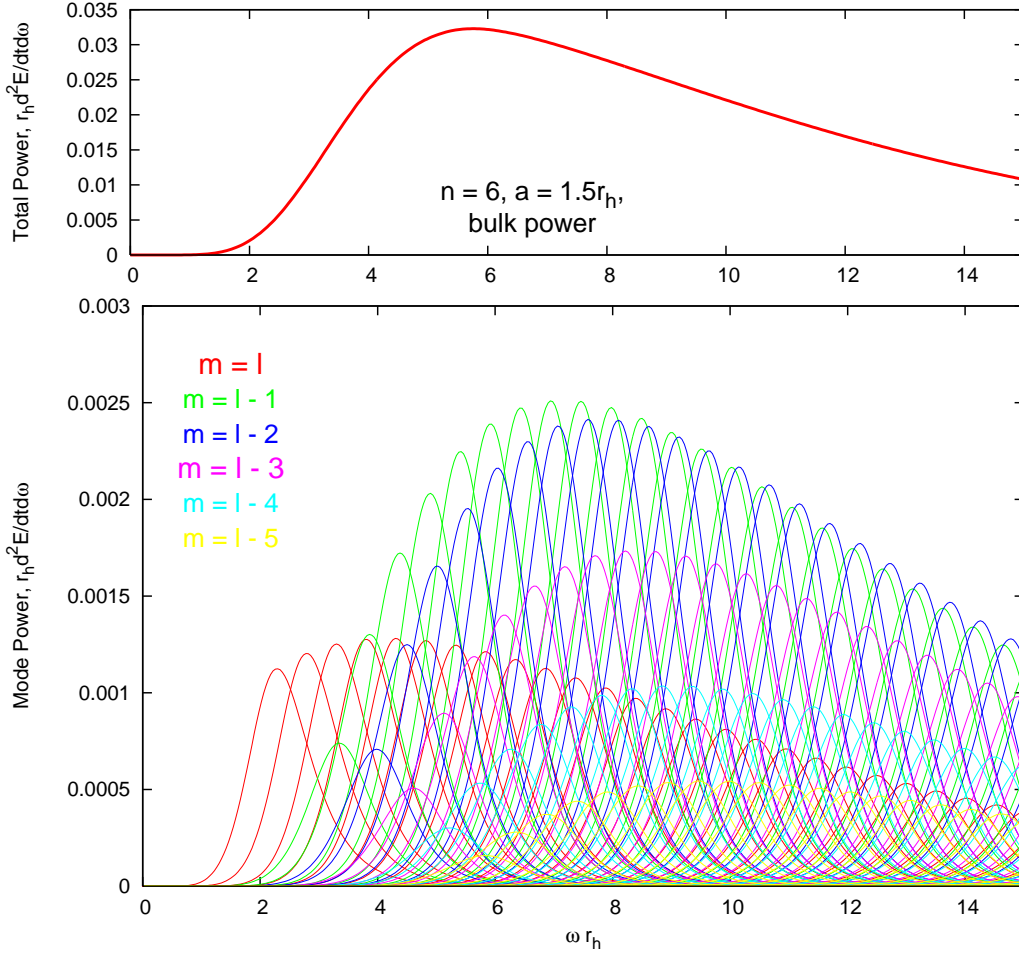


**Figure 9:** *Emission from a 10D black hole at  $a_d = 1.5$ .* The upper plot shows the total power. The lower plot shows the contribution from a ‘forest’ of modes,  $m = l$  to  $m = l - 5$ . It can be seen that the  $m = l$  modes are no longer dominant at all energies. Note that a sum over  $j$  has been taken where appropriate.

energetic than the black hole mass itself. For black holes created at a collider, we would expect the black hole mass to be only a few multiples of  $M_*$ . Many other physical effects may modify the spectrum for  $\omega r_h \gg 1$ . A concerted effort is currently underway to model the particle showers produced by black hole decay using Monte Carlo event generators [42].

Regardless of these physical considerations, it is still possible to compute an ‘idealised’ semi-classical emission spectra using equation (2.32). The calculation is easiest at low  $n$ , since many subdominant modes ( $m < l - m_{\text{cutoff}}$ ) can be neglected. Figure 12 shows bulk emission from a 5D black hole at  $a_d = 0, 1, 1.5, 2$  and  $3$ . Again, the oscillatory structure is due to the dominance of the superradiant ( $m = l$ ) modes. In every case we have studied we find the power spectrum reaches an overall peak and tends to zero as  $\omega r_h \rightarrow \infty$ .

#### 4.2.3 Angular momentum spectra

A rotating black hole loses both mass and angular momentum through the Hawking emis-

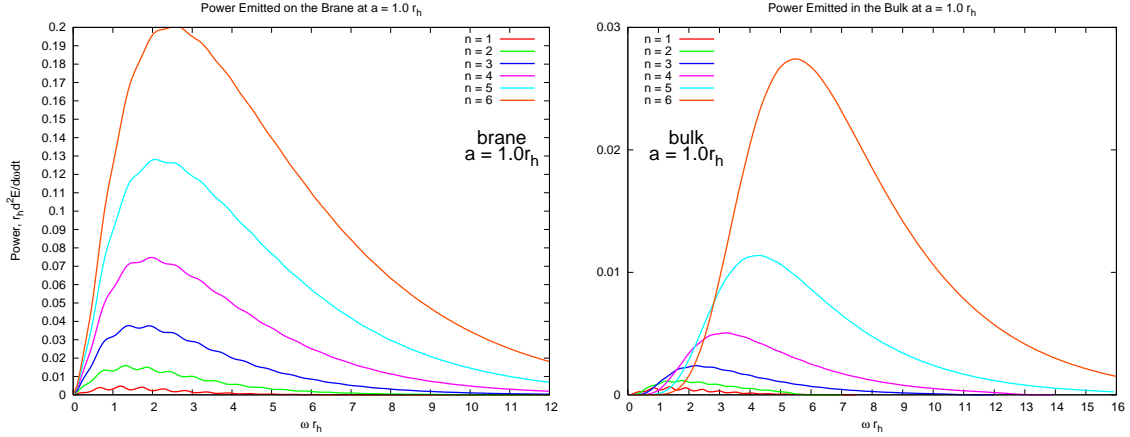


**Figure 10:** *Emission by a rotating black hole.* These plots compare the power emitted on the brane (left) and in the bulk (right) at  $a_d = 1.0$ . Note the difference in the scales on the  $y$ -axis.

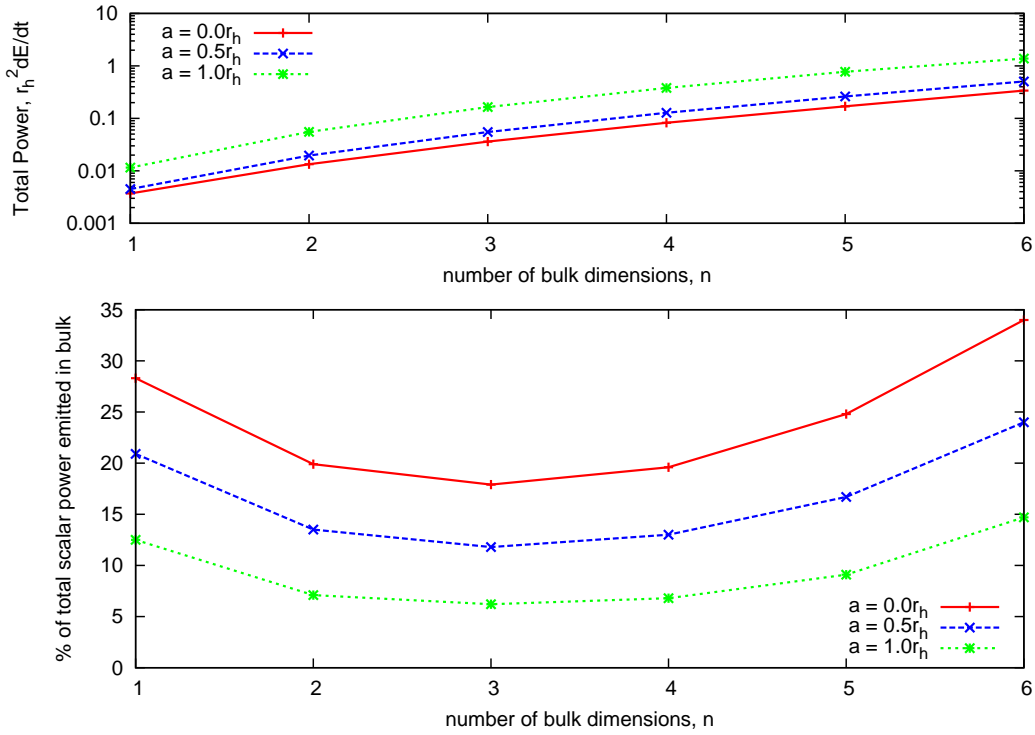


**Figure 11:** *Total scalar emission for a range of scenarios.* The upper plot shows the total power in brane and bulk scalars, for  $a_d = 0, 0.5$  and  $1$ , and for a range of numbers of extra dimensions,  $n = 1, 2 \dots 6$ . The lower plot shows the % of this power which is emitted into the bulk.

sion process. The loss rate of angular momentum is given by equation (2.33).

Figure 13 compares the loss rate of angular momentum on the brane (left panel) and in the bulk (right panel), for a range of rotations of a 6D ( $n = 2$ ) black hole. Note the order-of-magnitude difference in their magnitudes. Hence, the majority of angular momentum is

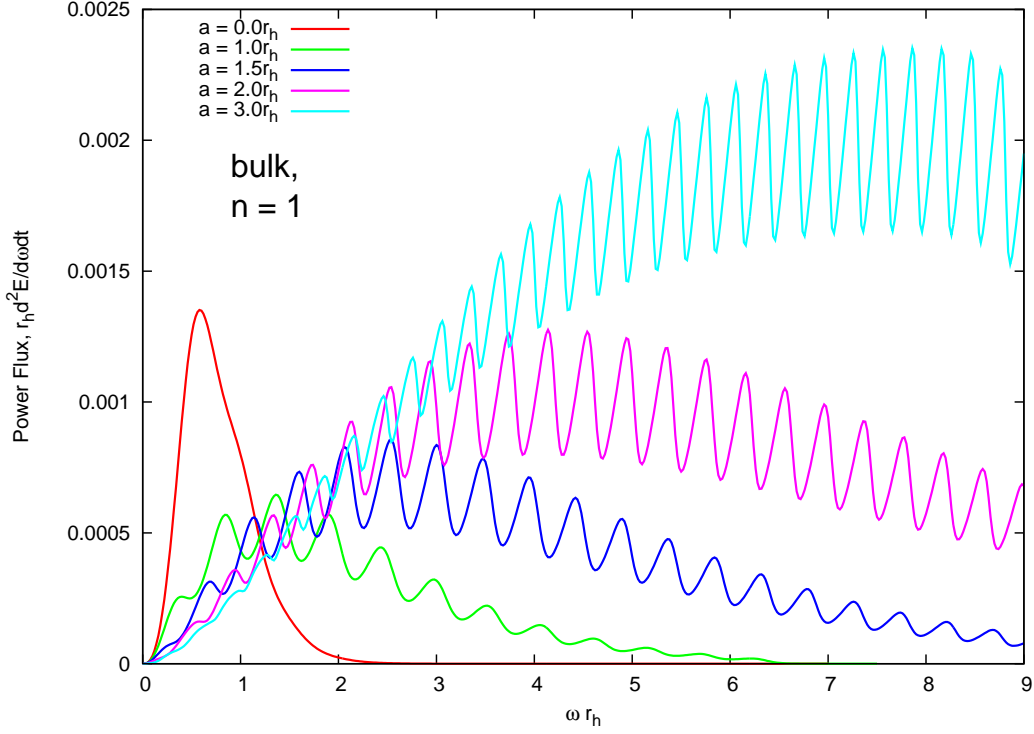


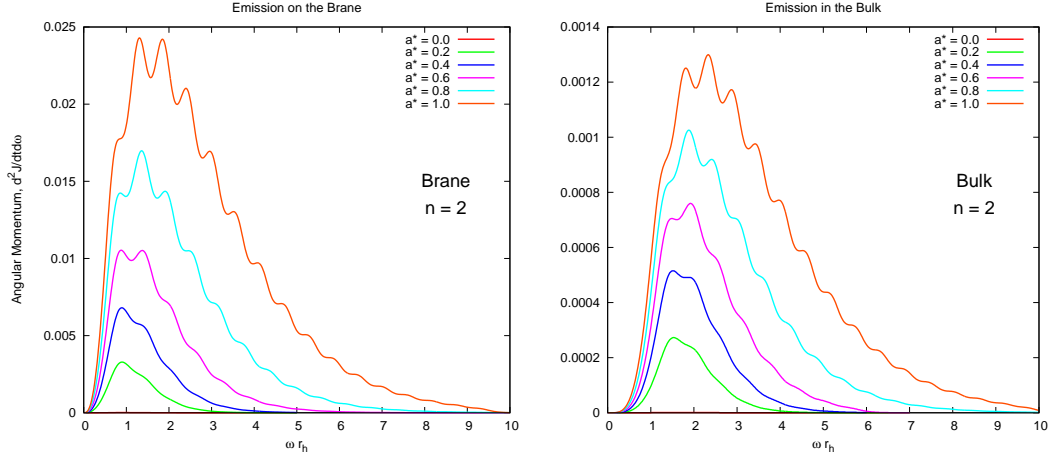
**Figure 12:** *Emission in the bulk from a fast-rotating 5D black hole.* The plot shows how the power emitted into the bulk varies with black hole rotation rate,  $a_d = a/r_h = 0, 1, 1.5, 2$  and  $3$ , with one extra dimension  $n = 1$ .

emitted on the brane. This is perhaps not surprising, since the plane of rotation lies on the brane. Table 4 lists the total angular momentum emission rates for  $n = 2$ ,  $a_d = 0 \dots 1.0$ . The proportion of angular momentum entering the bulk is found to decrease monotonically with  $a_d$ .

	$a_d = 0.2$	$a_d = 0.4$	$a_d = 0.6$	$a_d = 0.8$	$a_d = 1.0$
Bulk A.M.	$4.04 \times 10^{-4}$	$8.99 \times 10^{-4}$	$1.60 \times 10^{-3}$	$2.73 \times 10^{-3}$	$4.54 \times 10^{-3}$
Brane A.M.	$3.97 \times 10^{-3}$	$9.98 \times 10^{-3}$	$2.10 \times 10^{-2}$	$4.17 \times 10^{-2}$	$8.00 \times 10^{-2}$
% in Bulk	9.2%	8.3%	7.1%	6.1%	5.4%

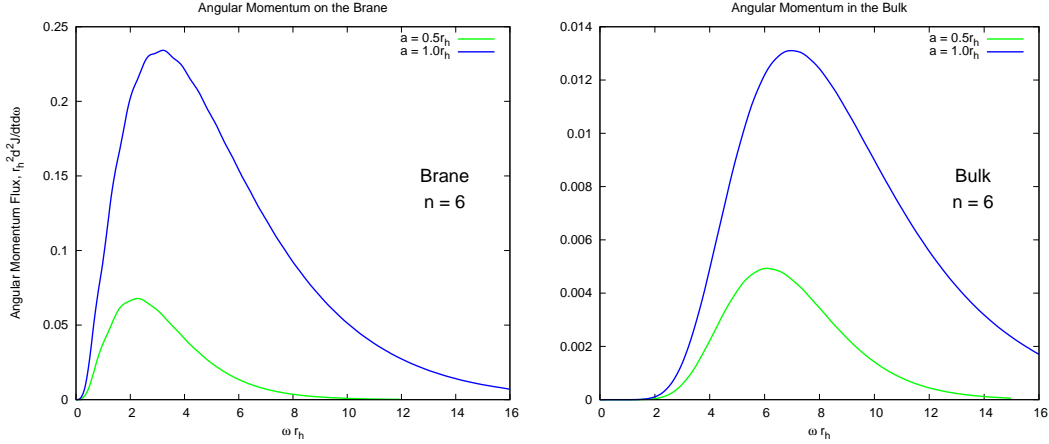
**Table 4:** *Proportion of (scalar) angular momentum emitted into the bulk by a 6D rotating black hole.* These figures were calculated by numerically integrating the angular momentum spectra, up to a cutoff of  $\omega r_h = 10$ . The angular momentum loss rate is given in units of  $1/r_h$ .

Figure 14 shows the angular momentum emitted by a rotating black hole embedded in a ten-dimensional bulk. Comparing with figure 13, we see that the overall emission rate has been enhanced by an order-of-magnitude by the increase in bulk dimensionality. We estimated the total angular momentum loss rate by integrating these spectra up to a cutoff of  $\omega r_h = 16$ . We found that, at  $a_d = 0.5$ , some 9.0% of the total angular momentum loss rate of  $0.28r_h^{-1}$  is emitted in the bulk. At  $a_d = 1.0$ , we estimate that 6.0% of a total of  $1.64r_h^{-1}$  is emitted in the bulk. Note that the latter estimate is an underestimate due to



**Figure 13:** *Brane and bulk angular momentum from a 6D rotating black hole.* The left and right plots show the angular momentum emitted on the brane and in the bulk, for a range of angular momenta  $a_d = a/r_h$ . Note the order-of-magnitude difference in the scales on the  $y$ -axis.

the integration cutoff (see figure 14).



**Figure 14:** *Brane and bulk angular momentum from a 10D rotating black hole.* The left and right plots show the angular momentum emitted on the brane and in the bulk, respectively. Note the order-of-magnitude difference in the scales on the  $y$ -axis.

### 4.3 Consistency with other studies

In this section we briefly compare our results with those published in the literature. We find our results are consistent with the previous studies, where comparison is possible. In all the papers mentioned below, the methods used to compute the greybody factors are different from those employed here, and therefore represent an independent check on our calculations.

First, let us consider the emission of scalars in the Schwarzschild phase. We find excellent agreement with the results presented in [12], for both brane and bulk emission,

although it should be emphasized that the numerical algorithms used in [12] are different from those we have used in section 3. The bulk-to-brane proportions in table 1 agree well with those in table 6 in [12] (to  $\sim 1$ ). We also find excellent agreement with the emission ratios presented in table 1 of the second paper in [13].

Next, let us consider scalar emission on the brane in the rotating phase; here, we are in agreement with [15], which again uses different numerical methodology to that in section 3. The total powers on the brane presented in table 3 are in reasonable agreement with the totals in figure 12b in [15]. Our values are likely to be more accurate than those shown in figure 12b of [15], because we use a higher cutoff frequency ( $\omega r_h \sim 16$  vs.  $\omega r_h \sim 3$ ).

We have checked the credibility of our new results for scalar emission in the bulk in a variety of ways. For example, in section 4 we confirmed that the numerical greybody factors agree with the analytic approximation derived in [19] in the appropriate limit ( $\omega r_h \lesssim l$ ). Comparison was also made with two numerical studies for the special cases  $n = 1$  and  $n = 2$  (i. e. 5D and 6D black holes). A study of bulk emission from a 6D rotating black hole lying on a tense brane was recently conducted in [21]. We confirmed with the authors that, when the brane tension is set to zero, our power spectra are in excellent agreement with their results (for the special cases  $n = 2$ ,  $a_d = 0, 0.6$  and  $1.2$ ). On the other hand, we cannot reproduce the results of a recent study of a 5D hole [20]; whilst we find good agreement for brane emission, we cannot verify their results for bulk emission (figure 5, [20]). Since this appears to be the only point of disagreement between our study and the existing literature, we remain confident that our numerical results are substantively correct.

## 5. Discussion and conclusions

The emission of Hawking radiation, in the form of elementary particles, by a higher-dimensional black hole might be the most distinctive signature of the creation of a black hole, and thus of the existence of extra dimensions in nature. Whereas the emission on the brane may in principle be directly observable and can be used as a source of valuable information about the extra dimensions, the emission in the bulk – the space transverse to our brane – will only be interpreted as a missing energy signal. Obviously, the more energy the black hole emits in the bulk, the less remains for emission on the brane. On the other hand, the amount of missing energy, due to the emission in the bulk and the emission of elusive particles such as neutrinos on the brane, is now considered as another distinctive signature of a black hole event. For the above reasons, the study of the emission in the bulk by a higher-dimensional black hole is of equal importance as the one on the brane.

The bulk emission channel for a higher-dimensional black hole in its spherically-symmetric Schwarzschild phase was the first one to be studied in the literature. Two types of particles are usually considered as being allowed to propagate in the bulk: gravitons and scalars. A comprehensive study for the case of the latter type of particles [12] demonstrated that the emission in the bulk remains always subdominant to the one on the brane, although it may become important for a large number of extra spacelike dimensions. A number of studies in the case of gravitons [13] have finally concluded that, although the emission of gravitons is enhanced by the existence of extra dimensions more than any other



species of particles, the total emission of gravitational modes remains subdominant to the one corresponding to the Standard Model degrees of freedom on the brane.

The study of the bulk emission during the spin-down phase of the life of the black hole has up to now been restricted to scalar fields. This is due to the increased complexity of the gravitational background around the rotating higher-dimensional black hole, and to the cumbersome formalism necessary to derive the equations of motion of higher-spin fields in the bulk. The existing scalar analyses themselves, although very illuminating, are either approximate [19] or refer to black holes with a specific dimensionality [20, 21]. For this reason, here we have attempted to present a comprehensive study of the bulk emission of scalar fields by a rotating black hole with arbitrary angular momentum and living in a spacetime with arbitrary number of extra dimensions.

The quantization of scalar fields propagating in a higher-dimensional, rotating black-hole background closely follows the one for their 4-dimensional analogues, therefore, in section 2 we have presented only the main steps of this analysis. It is worth mentioning that well-known techniques [33, 34, 35, 36, 37, 38, 40] developed for 4-dimensional space-time are found to hold also in this case leading to similar expressions for the energy and angular-momentum emission rates. Our numerical methods, used to compute the angular eigenvalues and the transmission factors, were described in detail in section 3. Finally, our exact numerical results for the bulk scalar emission from a rotating black hole were presented in section 4.

As a consistency check, our numerical analysis first reproduced the previously derived results for the emission of scalar fields by a non-rotating black hole in the bulk [12]. We then proceeded to study the rotating case, and demonstrated that the approximate analysis presented in [19] was in very good agreement with the exact numerical one in the low-energy regime. Inevitably, deviations appear beyond this regime, necessitating a full numerical study. The computation of the value of the transmission factor at all energies for a rotating black hole demands the consideration of a very large number of angular modes, that increases as the energy increases too. Our final results for the transmission factor revealed a hierarchical splitting of the modes according to the angular momentum numbers (first on  $l$ , then on  $m$ , and finally on  $j$ ) as well as the expected superradiance effect, that was most effective for the  $(m = l, j = 0)$  modes and for low values of  $n$ . Compared to the non-rotating case, the transmission factor for the most-dominant modes is found to be enhanced with the angular momentum of the black hole.

The corresponding power spectra for scalar fields were then computed. For the purpose of comparing bulk and brane emission, we derived both types of spectra for the same set of values of  $a$  and  $n$ . We find that whereas the brane scalar emission is enhanced with the angular momentum of the black hole, in accordance with previous studies, the bulk emission is initially suppressed and starts increasing only after a certain value of  $a$ . This effect persists for all values of  $n$  and is caused by the fact that – contrary to the emission on the brane – the enhancement of the transmission factor in the bulk is not in a position to compensate for the decrease in the black-hole temperature with  $a$ . The complete picture emerges from the entries of table 3, which lists the proportion of the total power emitted by the black hole in the bulk. From these, we see that, for all examined values of  $a$

and  $n$ , the bulk scalar emission is only a fraction of the brane emission. This fraction becomes important only for large values of  $n$ , as in the non-rotating case, and even then it is suppressed as  $a$  increases. We may thus safely conclude that, as far as the scalar channel is concerned, a rotating black hole emits a smaller fraction of its mass into the bulk than a non-rotating one. Our results therefore seem to add extra support to the argument presented in [22] that black holes radiate mainly on the brane.

Finally, we considered the angular-momentum loss rate of the black hole. Perhaps not surprisingly since the black hole's sole angular momentum component lies on the brane, we found again that the black hole loses its angular momentum mainly by emission on the brane rather than in the bulk. Thus, for the indicative case of a 6-dimensional black hole we found that the proportion of the angular momentum emitted in the bulk can be described with single figures, as can be seen in table 4.

The analysis of the brane-to-bulk energy balance is, however, not yet complete. The graviton emission channel for the rotating phase needs to be investigated before a final conclusion can be drawn. In the non-rotating case [13], it was found that the behaviour of the transmission factors for gravitons and scalar fields in the bulk shared a number of qualitative features, with the significant enhancement of the graviton power rate caused mainly by the larger number of degrees of freedom in the bulk. It remains to be seen whether, for a rotating black hole, the graviton transmission factors will exhibit the same characteristics as the scalar transmission factors found in this work. If so, it also remains to be seen whether the number of graviton states can tilt the balance towards bulk emission. For this, we would need the perturbed equation of motion for gravitons in a general rotating, higher-dimensional black-hole background which is unfortunately still missing from the literature.

## Acknowledgments

M.C. wishes to acknowledge Science Foundation Ireland for financial support. S.D. acknowledges financial support from the Irish Research Council for Science, Engineering and Technology (IRCSET). P.K. and E.W. wish to thank University College Dublin for hospitality during the early stages of this work. P.K. also acknowledges financial support from the UK STFC PPA/A/S/2002/00350 research grant and participation in the RTN networks UNIVERSENET-MRTN-CT-2006-035863-1 and MRTN-CT-2004-503369. The work of E.W. was supported by UK STFC, grant numbers PPA/G/S/2003/00082 and PPA/D000351/1.

## References

- [1] N. Arkani-Hamed, S. Dimopoulos and G. R. Dvali, *The hierarchy problem and new dimensions at a millimeter*, *Phys. Lett. B* **429** (1998) 263 [[hep-ph/9803315](#)];  
*Phenomenology, astrophysics and cosmology of theories with sub-millimeter dimensions and TeV scale quantum gravity*, *Phys. Rev. D* **59** (1999) 086004 [[hep-ph/9807344](#)];

- I. Antoniadis, N. Arkani-Hamed, S. Dimopoulos and G. R. Dvali, *New dimensions at a millimeter to a Fermi and superstrings at a TeV*, *Phys. Lett. B* **436** (1998) 257 [[hep-ph/9804398](#)].
- [2] L. Randall and R. Sundrum, *A large mass hierarchy from a small extra dimension*, *Phys. Rev. Lett.* **83** (1999) 3370 [[hep-ph/9905221](#)]; *An alternative to compactification*, *Phys. Rev. Lett.* **83** (1999) 4690 [[hep-ph/9906064](#)].
- [3] T. Banks and W. Fischler, *A model for high-energy scattering in quantum gravity*, [hep-th/9906038](#);  
D. M. Eardley and S. B. Giddings, *Classical black hole production in high-energy collisions*, *Phys. Rev. D* **66** (2002) 044011 [[gr-qc/0201034](#)];  
H. Yoshino and Y. Nambu, *High-energy head-on collisions of particles and hoop conjecture*, *Phys. Rev. D* **66** (2002) 065004 [[gr-qc/0204060](#)]; *Black hole formation in the grazing collision of high-energy particles*, *Phys. Rev. D* **67** (2003) 024009 [[gr-qc/0209003](#)];  
E. Kohlprath and G. Veneziano, *Black holes from high-energy beam-beam collisions*, *J. High Energy Phys.* **06** (2002) 057 [[gr-qc/0203093](#)];  
V. Cardoso, O. J. C. Dias and J. P. S. Lemos, *Gravitational radiation in D-dimensional spacetimes*, *Phys. Rev. D* **67** (2003) 064026 [[hep-th/0212168](#)];  
E. Berti, M. Cavaglià and L. Gualtieri, *Gravitational energy loss in high energy particle collisions: Ultrarelativistic plunge into a multidimensional black hole*, *Phys. Rev. D* **69** (2004) 124011 [[hep-th/0309203](#)];  
V. S. Rychkov, *Black hole production in particle collisions and higher curvature gravity*, *Phys. Rev. D* **70** (2004) 044003 [[hep-ph/0401116](#)];  
S. B. Giddings and V. S. Rychkov, *Black holes from colliding wavepackets*, *Phys. Rev. D* **70** (2004) 104026 [[hep-th/0409131](#)];  
O. I. Vasilenko, *Trap surface formation in high-energy black holes collision*, [hep-th/0305067](#);  
H. Yoshino and V. S. Rychkov, *Improved analysis of black hole formation in high-energy particle collisions*, *Phys. Rev. D* **71** (2005) 104028 [[hep-th/0503171](#)];  
D. C. Dai, G. D. Starkman and D. Stojkovic, *Production of black holes and their angular momentum distribution in models with split fermions*, *Phys. Rev. D* **73** (2006) 104037 [[hep-ph/0605085](#)];  
H. Yoshino and R. B. Mann, *Black hole formation in the head-on collision of ultrarelativistic charges*, *Phys. Rev. D* **74** (2006) 044003 [[gr-qc/0605131](#)].
- [4] A. Goyal, A. Gupta and N. Mahajan, *Neutrinos as source of ultra high-energy cosmic rays in extra dimensions*, *Phys. Rev. D* **63** (2001) 043003 [[hep-ph/0005030](#)];  
J. L. Feng and A. D. Shapere, *Black hole production by cosmic rays*, *Phys. Rev. Lett.* **88** (2002) 021303 [[hep-ph/0109106](#)];  
L. Anchordoqui and H. Goldberg, *Experimental signature for black hole production in neutrino air showers*, *Phys. Rev. D* **65** (2002) 047502 [[hep-ph/0109242](#)];  
R. Emparan, M. Masip and R. Rattazzi, *Cosmic rays as probes of large extra dimensions and TeV gravity*, *Phys. Rev. D* **65** (2002) 064023 [[hep-ph/0109287](#)];  
L. A. Anchordoqui, J. L. Feng, H. Goldberg and A. D. Shapere, *Black holes from cosmic rays: Probes of extra dimensions and new limits on TeV-scale gravity*, *Phys. Rev. D* **65** (2002) 124027 [[hep-ph/0112247](#)]; *Updated limits on TeV scale gravity from absence of neutrino cosmic ray showers mediated by black holes*, *Phys. Rev. D* **68** (2003) 104025 [[hep-ph/0307228](#)];  
Y. Uehara, *Production and detection of black holes at neutrino array*, *Prog. Theor. Phys.* **107** (2002) 621 [[hep-ph/0110382](#)];

- J. Alvarez-Muñiz, J. L. Feng, F. Halzen, T. Han and D. Hooper, *Detecting microscopic black holes with neutrino telescopes*, *Phys. Rev. D* **65** (2002) 124015 [[hep-ph/0202081](#)];
- A. Ringwald and H. Tu, *Collider versus cosmic ray sensitivity to black hole production*, *Phys. Lett. B* **525** (2002) 135 [[hep-ph/0111042](#)];
- M. Kowalski, A. Ringwald and H. Tu, *Black holes at neutrino telescopes*, *Phys. Lett. B* **529** (2002) 1 [[hep-ph/0111042](#)];
- E. J. Ahn, M. Ave, M. Cavaglià and A. V. Olinto, *TeV black hole fragmentation and detectability in extensive air-showers*, *Phys. Rev. D* **68** (2003) 043004 [[hep-ph/0306008](#)];
- E. J. Ahn, M. Cavaglià and A. V. Olinto, *Uncertainties in limits on TeV-gravity from neutrino induced air showers*, *Astropart. Phys.* **22** (2005) 377 [[hep-ph/0312249](#)];
- T. Han and D. Hooper, *The particle physics reach of high-energy neutrino astronomy*, *New J. Phys.* **6** (2004) 150 [[hep-ph/0408348](#)];
- A. Cafarella, C. Coriano and T. N. Tomaras, *Cosmic ray signals from mini black holes in models with extra dimensions: An analytical / Monte Carlo study*, *J. High Energy Phys.* **06** (2005) 065 [[hep-ph/0410358](#)];
- D. Stojkovic and G. D. Starkman, *Why black hole production in scattering of cosmic ray neutrinos is generically suppressed*, *Phys. Rev. Lett.* **96** (2006) 041303 [[hep-ph/0505112](#)];
- A. Barrau, C. Feron and J. Grain, *Astrophysical production of microscopic black holes in a low Planck-scale world*, *Astrophys. J.* **630** (2005) 1015 [[astro-ph/0505436](#)];
- L. Anchordoqui, T. Han, D. Hooper and S. Sarkar, *Exotic neutrino interactions at the Pierre Auger observatory*, *Astropart. Phys.* **25** (2006) 14 [[hep-ph/0508312](#)];
- E. J. Ahn and M. Cavaglià, *Simulations of black hole air showers in cosmic ray detectors*, *Phys. Rev. D* **73** (2006) 042002 [[hep-ph/0511159](#)].
- [5] S. B. Giddings and S. Thomas, *High energy colliders as black hole factories: The end of short distance physics*, *Phys. Rev. D* **65** (2002) 056010 [[hep-ph/0106219](#)];
- S. Dimopoulos and G. Landsberg, *Black holes at the LHC*, *Phys. Rev. Lett.* **87** (2001) 161602 [[hep-ph/0106295](#)];
- S. Dimopoulos and R. Emparan, *String balls at the LHC and beyond*, *Phys. Lett. B* **526** (2002) 393 [[hep-ph/0108060](#)];
- S. Hossenfelder, S. Hofmann, M. Bleicher and H. Stöcker, *Quasi-stable black holes at LHC*, *Phys. Rev. D* **66** (2002) 101502 [[hep-ph/0109085](#)];
- K. Cheung, *Black hole production and large extra dimensions*, *Phys. Rev. Lett.* **88** (2002) 221602 [[hep-ph/0110163](#)];
- R. Casadio and B. Harms, *Can black holes and naked singularities be detected in accelerators?*, *Int. J. Mod. Phys. A* **17** (2002) 4635 [[hep-ph/0110255](#)];
- S. C. Park and H. S. Song, *Production of spinning black holes at colliders*, *J. Korean Phys. Soc.* **43** (2003) 30 [[hep-ph/0111069](#)];
- G. Landsberg, *Discovering new physics in the decays of black holes*, *Phys. Rev. Lett.* **88** (2002) 181801 [[hep-ph/0112061](#)];
- G. F. Giudice, R. Rattazzi and J. D. Wells, *Transplanckian collisions at the LHC and beyond*, *Nucl. Phys. B* **630** (2002) 293 [[hep-ph/0112161](#)];
- E. J. Ahn, M. Cavaglià and A. V. Olinto, *Brane factories*, *Phys. Lett. B* **551** (2003) 1 [[hep-th/0201042](#)];
- A. Mironov, A. Morozov and T. N. Tomaras, *Can centauros or chirons be the first observations of evaporating mini black holes?*, [hep-ph/0311318](#);
- T. G. Rizzo, *Black hole production at the LHC: effects of Voloshin suppression*, *J. High Energy Phys.* **02** (2002) 011 [[hep-ph/0201228](#)]; *Warped phenomenology of higher-derivative gravity*, *J. High Energy Phys.* **01** (2005) 025 [[hep-ph/0412087](#)];

- A. V. Kotwal and C. Hays, *Production and decay of spinning black holes at colliders and tests of black hole dynamics*, *Phys. Rev. D* **66** (2002) 116005 [[hep-ph/0206055](#)];
- A. Chamblin and G. C. Nayak, *Black hole production at LHC: String balls and black holes from  $pp$  and lead-lead collisions*, *Phys. Rev. D* **66** (2002) 091901 [[hep-ph/0206060](#)];
- T. Han, G. D. Kribs and B. McElrath, *Black hole evaporation with separated fermions*, *Phys. Rev. Lett.* **90** (2003) 031601 [[hep-ph/0207003](#)];
- I. Mocioiu, Y. Nara and I. Sarcevic, *Hadrons as signature of black hole production at the LHC*, *Phys. Lett. B* **557** (2003) 87 [[hep-ph/0310073](#)];
- M. Cavaglià, S. Das and R. Maartens, *Will we observe black holes at LHC?*, *Class. and Quant. Grav.* **20** (2003) L205 [[hep-ph/0305223](#)];
- D. Stojkovic, *Distinguishing between the small ADD and RS black holes in accelerators*, *Phys. Rev. Lett.* **94** (2005) 011603 [[hep-ph/0409124](#)];
- S. Hossenfelder, *The minimal length and large extra dimensions*, *Mod. Phys. Lett. A* **19** (2004) 2727 [[hep-ph/0410122](#)];
- C. M. Harris, M. J. Palmer, M. A. Parker, P. Richardson, A. Sabetfakhri and B. R. Webber, *Exploring higher dimensional black holes at the Large Hadron Collider*, *J. High Energy Phys.* **05** (2005) 053 [[hep-ph/0411022](#)];
- G. L. Alberghi, R. Casadio, D. Galli, D. Gregori, A. Tronconi and V. Vagnoni, *Probing quantum gravity effects in black holes at LHC*, [hep-ph/0601243](#);
- G. C. Nayak and J. Smith, *Higgs boson production from black holes at the LHC*, *Phys. Rev. D* **74** (2006) 014007 [[hep-ph/0602129](#)];
- H. Stocker, *Stable TeV - black hole remnants at the LHC: Discovery through di-jet suppression, mono-jet emission and a supersonic boom in the quark-gluon plasma*, *Int. J. Mod. Phys. D* **16** (2007) 185 [[hep-ph/0605062](#)];
- L. Lonnblad and M. Sjodahl, *Classical and non-classical ADD-phenomenology with high- $E(T)$  jet observables at collider experiments*, *J. High Energy Phys.* **10** (2006) 088 [[hep-ph/0608210](#)].
- [6] S. W. Hawking, *Particle creation by black holes*, *Commun. Math. Phys.* **43** (1975) 199.
- [7] P. Kanti, *Black holes in theories with large extra dimensions: A review*, *Int. J. Mod. Phys. A* **19** (2004) 4899 [[hep-ph/0402168](#)].
- [8] M. Cavaglià, *Black hole and brane production in TeV gravity: A review*, *Int. J. Mod. Phys. A* **18** (2003) 1843 [[hep-ph/0210296](#)];
- G. Landsberg, *Black holes at future colliders and in cosmic rays*, *Eur. Phys. J. C* **33** (2004) S927 [[hep-ex/0310034](#)];
- A. S. Majumdar and N. Mukherjee, *Braneworld black holes in cosmology and astrophysics*, *Int. J. Mod. Phys. D* **14** (2005) 1095 [[astro-ph/0503473](#)];
- A. Casanova and E. Spallucci, *TeV mini black hole decay at future colliders*, *Class. and Quant. Grav.* **23** (2006) R45 [[hep-ph/0512063](#)];
- E. Winstanley, *Hawking radiation from rotating brane black holes*, [arXiv:0708.2656](#) [[hep-th](#)];
- P. Kanti, *Black holes at the LHC*, [arXiv:0802.2218](#) [[hep-th](#)].
- [9] P. Kanti and J. March-Russell, *Calculable corrections to brane black hole decay. I: The scalar case*, *Phys. Rev. D* **66** (2002) 024023 [[hep-ph/0203223](#)].
- [10] V. P. Frolov and D. Stojkovic, *Black hole radiation in the brane world and recoil effect*, *Phys. Rev. D* **66** (2002) 084002 [[hep-th/0206046](#)].

- [11] P. Kanti and J. March-Russell, *Calculable corrections to brane black hole decay. II: Greybody factors for spin 1/2 and 1*, *Phys. Rev. D* **67** (2003) 104019 [[hep-ph/0212199](#)].
- [12] C. M. Harris and P. Kanti, *Hawking radiation from a  $(4+n)$ -dimensional black hole: Exact results for the Schwarzschild phase*, *J. High Energy Phys.* **10** (2003) 014 [[hep-ph/0309054](#)].
- [13] V. Cardoso, M. Cavaglià and L. Gualtieri, *Black hole particle emission in higher-dimensional spacetimes*, *Phys. Rev. Lett.* **96** (2006) 071301 [[hep-th/0512002](#)]; *Hawking emission of gravitons in higher dimensions: non-rotating black holes*, *J. High Energy Phys.* **02** (2006) 021 [[hep-th/0512116](#)];  
S. Creek, O. Efthimiou, P. Kanti and K. Tamvakis, *Graviton emission in the bulk from a higher-dimensional Schwarzschild black hole*, *Phys. Lett. B* **635** (2006) 39 [[hep-th/0601126](#)];  
A. S. Cornell, W. Naylor and M. Sasaki, *Graviton emission from a higher-dimensional black hole*, *J. High Energy Phys.* **02** (2006) 012 [[hep-th/0510009](#)].
- [14] V. P. Frolov and D. Stojkovic, *Quantum radiation from a 5-dimensional rotating black hole*, *Phys. Rev. D* **67** (2003) 084004 [[gr-qc/0211055](#)].
- [15] G. Duffy, C. Harris, P. Kanti and E. Winstanley, *Brane decay of a  $(4+n)$ -dimensional rotating black hole: spin-0 particles*, *J. High Energy Phys.* **09** (2005) 049 [[hep-th/0507274](#)].
- [16] M. Casals, P. Kanti and E. Winstanley, *Brane decay of a  $(4+n)$ -dimensional rotating black hole. II: spin-1 particles*, *J. High Energy Phys.* **02** (2006) 051 [[hep-th/0511163](#)].
- [17] M. Casals, S. R. Dolan, P. Kanti and E. Winstanley, *Brane decay of a  $(4+n)$ -dimensional rotating black hole. III: spin-1/2 particles*, *J. High Energy Phys.* **03** (2007) 019 [[hep-th/0608193](#)].
- [18] D. Ida, K. y. Oda and S. C. Park, *Rotating black holes at future colliders: Greybody factors for brane fields*, *Phys. Rev. D* **67** (2003) 064025 [Erratum: *ibid.* **69** (2004) 049901] [[hep-th/0212108](#)]; *Rotating black holes at future colliders. II: Anisotropic scalar field emission*, *Phys. Rev. D* **71** (2005) 124039 [[hep-th/0503052](#)]; *Rotating black holes at future colliders. III: Determination of black hole evolution*, *Phys. Rev. D* **73** (2006) 124022 [[hep-th/0602188](#)].
- [19] S. Creek, O. Efthimiou, P. Kanti and K. Tamvakis, *Scalar emission in the bulk in a rotating black hole background*, *Phys. Lett. B* **656** (2007) 102 [[arXiv:0709.0241](#) [[hep-th](#)]].
- [20] E. Jung and D. K. Park, *Bulk versus brane in the absorption and emission: 5d rotating black hole case*, *Nucl. Phys. B* **731** (2005) 171 [[hep-th/0506204](#)].
- [21] T. Kobayashi, M. Nozawa, Y. Takamizu, *Bulk scalar emission from a rotating black hole pierced by a tense brane*, *Phys. Rev. D* **77** (2008) 044022 [[arXiv:0711.1395](#) [[hep-th](#)]].
- [22] R. Emparan, G. T. Horowitz and R. C. Myers, *Black holes radiate mainly on the brane*, *Phys. Rev. Lett.* **85** (2000) 499 [[hep-th/0003118](#)].
- [23] H. Kodama, *Perturbations and stability of higher-dimensional black holes*, [arXiv:0712.2703](#) [[hep-th](#)]; *Superradiance and instability of black holes*, [arXiv:0711.4184](#) [[hep-th](#)].
- [24] H. K. Kunduri, J. Lucietti and H. S. Reall, *Gravitational perturbations of higher dimensional rotating black holes: tensor perturbations*, *Phys. Rev. D* **74** (2006) 084021 [[hep-th/0606076](#)].
- [25] K. Murata and J. Soda, *A note on separability of field equations in Myers-Perry spacetimes*, *Class. and Quant. Grav.* **25** (2008) 035006 [[arXiv:0710.0221](#) [[hep-th](#)]].

- [26] R. C. Myers and M. J. Perry, *Black holes in higher dimensional space-times*, *Ann. Phys. (NY)* **172** (1986) 304.
- [27] C. M. Harris, *Physics beyond the standard model: exotic leptons and black holes at future colliders*, [hep-ph/0502005](#).
- [28] C. Muller, *Lecture Notes in Mathematics: Spherical Harmonics* (Springer-Verlag, Berlin-Heidelberg, 1966).
- [29] E. Berti, V. Cardoso, M. Casals, *Eigenvalues and eigenfunctions of spin-weighted spheroidal harmonics in four and higher dimensions*, *Phys. Rev. D* **73** (2006) 024013 [[gr-qc/0511111](#)].
- [30] E. W. Leaver, *An analytic representation for the quasi-normal modes of Kerr black holes*, *Proc. R. Soc. London A* **402** (1985) 285.
- [31] A. C. Ottewill and E. Winstanley, *Renormalized stress tensor in Kerr space-time: General results*, *Phys. Rev. D* **62** (2002) 084018 [[gr-qc/0004022](#)].
- [32] M. Casals and A. C. Ottewill, *Canonical quantization of the electromagnetic field on the Kerr background*, *Phys. Rev. D* **71** (2005) 124016 [[gr-qc/0501005](#)].
- [33] V. P. Frolov and K. S. Thorne, *Renormalized stress-energy tensor near the horizon of a slowly evolving, rotating black hole*, *Phys. Rev. D* **39** (1989) 2125.
- [34] W. G. Unruh, *Notes on black-hole evaporation*, *Phys. Rev. D* **14** (1976) 870.
- [35] S. M. Christensen, *Vacuum expectation value of the stress tensor in an arbitrary curved background: The covariant point-separation method*, *Phys. Rev. D* **14** (1976) 2490.
- [36] S. M. Christensen, *Regularization, renormalization, and covariant geodesic point separation*, *Phys. Rev. D* **17** (1978) 946.
- [37] B. S. DeWitt, *The dynamical theory of groups and fields* (Gordon and Breach, New York, 1965).
- [38] J. Schwinger, *On gauge invariance and vacuum polarization*, *Phys. Rev.* **82** (1951) 664.
- [39] V. P. Frolov, F. D. Mazzitelli and J. P. Paz, *Quantum effects near multidimensional black holes*, *Phys. Rev. D* **40** (1989) 948.
- [40] J. L. Synge, *Relativity: the general theory* (North-Holland, Amsterdam, 1960).
- [41] M. Casals and A. C. Ottewill, *High frequency asymptotics for the spin-weighted spheroidal equation*, *Phys. Rev. D* **71** (2005) 064025 [[gr-qc/0409012](#)].
- [42] C. M. Harris, P. Richardson and B. R. Webber, *CHARYBDIS: A black hole event generator*, *J. High Energy Phys.* **08** (2003) 033 [[hep-ph/0307305](#)];  
M. Cavaglià, R. Godang, L. Cremaldi and D. Summers, *Catfish: A Monte Carlo simulator for black holes at the LHC*, *Comput. Phys. Commun.* **177** (2007) 506 [[hep-ph/0609001](#)];  
D-C. Dai, G. Starkman, D. Stojkovic, C. Issever, E. Rizvi, and J. Tseng, *BlackMax: A black-hole event generator with rotation, recoil, split branes and brane tension*, *Phys. Rev. D* **77** (2008) 076007 [[arXiv:0711.3012](#) [[hep-ph](#)]].